# Supporting Information for:

# Rosette Nanotubes with 1.4 nm Inner Diameter from a Tricyclic Variant of the Lehn–Mascal G∧C Base

**Gabor Borzsonyi,[a,b] Ross S. Johnson,[a,b] Andrew J. Myles,[b] Jay-Young Cho,[b] Takeshi Yamazaki,[b] Rachel L. Beingessner, Andriy Kovalenko,[b,c] and Hicham Fenniri*[,a,b]**

[a] *Department of Chemistry, 11227 Saskatchewan Drive, University of Alberta, Edmonton, Alberta, T6G 2G2, Canada.*
[b] *National Institute for Nanotechnology, 11421 Saskatchewan Drive, University of Alberta, Edmonton, Alberta, T6G 2M9, Canada.*
[c] *Department of Mechanical Engineering, 4–9 Mechanical Engineering Building, University of Alberta, Edmonton, Alberta, T6G 2G8, Canada.*
*Fax: 780-641-1601; Tel: 780-641-1750; E-mail: hicham.fenniri@ualberta.ca*

## Abbreviations

ACN (acetonitrile); AFM (atomic force microscopy); app (apparent); Bn (benzyl); Boc (*tert*–butyloxycarbonyl); br (broad); d (doublet); $CHCl_3$ (chloroform); DCM (dichloromethane); $dH_2O$ (deionized NanoPure water); DIEA (diisopropylethylamine); DMAP (4–N,N dimethylaminopyridine); EA (elemental analysis); EtOAc (ethylacetate); DMF (N,N–dimethylformamide); DMSO (dimethylsulfoxide); ESI–MS (electrospray ionization mass spectrometry); $Et_3N$ (triethylamine); h (hour); HCl (hydrochloric acid); m (multiplet); m.p. (melting point); MeOH (methanol); min (minute); NMR (nuclear magnetic resonance); q (quartet); $R_f$ (retention factor); rt (room temperature); s (singlet); sat (saturated); SEM (scanning electron microscopy); t (triplet); *t*–Bu (*tert*–butyl); TEM (transmission electron microscopy); TFAA (trifluoroacetic anhydride); THF (tetrahydrofuran); TLC (thin layer chromatography).

## General

All the reagents and solvents are commercially available from Aldrich, Novabiochem, BaChem, Fluka, or Fisher Scientific, and were used without further purification. Compound **1** was synthesized following our previously reported procedure.[1] Reagent grade ACN, DCM and THF

were purified on an MBraun solvent purification system. For column chromatography, commercial solvents were used without purification. Chromatographic supports were silica flash Merck 60 (0.040–0.063 mm) or silica gel Merck 60 (0.063–0.2 mm) for gravity chromatography. Silica–coated TLC plates (Merck F 60254) were used for monitoring reaction progress.

$^{1}$H and $^{13}$C–NMR spectra were recorded on Varian Inova NMR spectrometers (400, 500, or 600 MHz) with the solvent as internal reference. The NMR data is presented as follows: chemical shift, peak assignment, multiplicity, coupling constant, integration. Assignments were made from 2D–NMR techniques (COSY, TROESY, HMBC, HMQC). The mass spectra were performed at the Mass Spectrometry Laboratory at the Department of Chemistry, University of Alberta, or in the Analytical Laboratory of The National Institute for Nanotechnology, University of Alberta.

## Synthesis

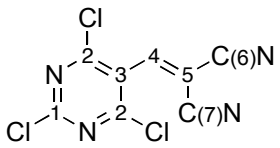


**Synthesis of compound 2.** Compound **1**[1] (18 g, 87 mmol) was dissolved in anhydrous ACN (180 mL) at rt under $N_2$ atmosphere. β–alanine (7.6 g, 87 mmol) and malonitrile (6.3 g, 95 mmol) were added and the mixture was stirred at rt for 30 h under $N_2$ atmosphere. The reaction was quenched with $dH_2O$ (500 mL) and compound **2** was filtered-off, recrystallized from toluene and further purified by silica gel flash chromatography (30% EtOAc/hexane) to yield compound **2** as a white solid ($C_8HCl_3N_4$, 11.0 g, 50%). $R_f$ = 0.6 (10% EtOAc/Hexane). mp = 158–160ºC.

$^{1}$H–NMR (600 MHz, $CDCl_3$) δ (ppm): 7.81 (C4H, sharp s, 1H).

$^{13}$C–NMR (150 MHz, $CDCl_3$) δ (ppm): 161.7, 161.3 (C1, C2), 150.5 (C4), 122.6 (C3), 110.9, 109.7 (C6, C7), 96.5 (C5).

Positive ESI–MS: Expected mass for m/z, 257.9. Observed, 258.6 [$(M+H^+)/z$].

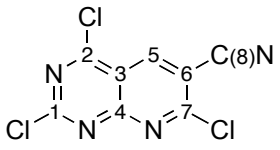


**Synthesis of compound 3.** Compound **2** (1.0 g, 3.9 mmol) was heated at 180ºC in a round bottom flask equipped with a $CaSO_4$ drying tube for two days in an oven. Sublimation of the crude mixture (0.1 mbar, 180ºC) yielded analytically pure compound **3** ($C_8HCl_3N_4$, 0.8 g, 75%). $R_f$ = 0.5 (10% EtOAc/Hexane). mp = 185–187ºC.

$^1$H–NMR (500 MHz, $CDCl_3$) δ (ppm): 8.96 (C5H, sharp s, 1H).

$^{13}$C–NMR (125 MHz, $CDCl_3$) δ (ppm): 164.9, 163.1 (C1, C4), 159.6, 159.1 (C2, C7), 143.4 (C5), 115.8, 113.1, 112.0 (C3, C6, C8).

Positive ESI–MS: Expected mass for m/z, 257.9. Observed, 258.6 [(M+H$^+$)/z].

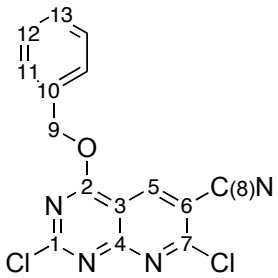


**Synthesis of compound 4.** Compound **3** (0.7 g, 2.73 mmol) was dissolved in anhydrous DCM (35 mL) at rt under $N_2$ atmosphere. The solution was cooled to –40ºC and a mixture of anhydrous $Et_3N$ (0.42 mL, 3.0 mmol) and benzyl alcohol (0.26 mL, 2.8 mmol) was added dropwise. The reaction mixture was stirred for 2 h under $N_2$ atmosphere at –40ºC. The solvent was evaporated (rotovap) and the residue was recrystallized from anhydrous $CHCl_3$/hexane to yield compound **4** ($C_{15}H_8Cl_2N_4O$, 0.59 g, 70%). mp = 216–218ºC.

$^1$H–NMR (600 MHz, $CDCl_3$) δ (ppm): 8.80 (C5H, sharp s, 1H), 7.53–7.42 (C11–13H, m, 5H), 5.70 (C9H, s, 2H).

$^{13}$C–NMR (150 MHz, $CDCl_3$) δ (ppm): 167.9, 164.1, 160.3, 158.0 (C1, C2, C4, C7), 141.7 (C5), 133.6 (C10), 129.5, 129.2, 129.0 (C11, C12, C13), 113.7, 109.7, 108.1 (C3, C6, C8), 71.9 (C9).

Positive ESI–MS: Expected mass for m/z, 330.0. Observed, 331.5 [(M+H$^+$)/z].

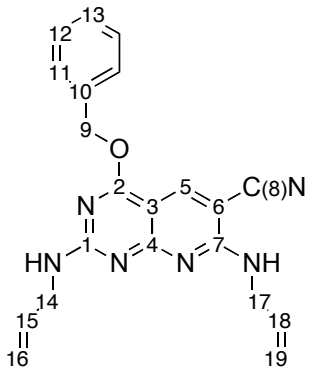

**Synthesis of compound 5.** Compound **4** (0.32 g, 0.97 mmol) was dissolved in anhydrous DCM (20 mL) under $N_2$ atmosphere. To this solution was added anhydrous allylamine (0.64 mL, 4.6 mmol) in anhydrous DCM (0.5 mL). The mixture was heated to 50ºC in a sealed tube and stirred for 15 h. The solvent was evaporated (rotovap) and the residue was purified by silica gel column chromatography (0–0.5% MeOH/DCM). Recrystallization from EtOAc yielded pure compound **5** ($C_{21}H_{20}N_6O$, 0.32 g, 89%). mp = 225–227ºC.

$^1$H–NMR (500 MHz, DMSO-*d*$_6$, 90ºC) δ (ppm): 8.28 (C5H, sharp s, 1H), 7.60–7.55 (NH, br s, 1H), 7.55–7.50 (C11H, m, 2H), 7.45–7.35 (C12H and C13H, m, 3H), 7.35–7.31 (NH, br s, 1H), 6.02–5.90 (C15H and C18H, m, 2H), 5.55 (C9H, s, 2H), 5.28–5.05 (C16H and C19H, m, 4H), 4.20–4.05 (C14H and C17H, m, 4H).

$^{13}$C–NMR (125 MHz, DMSO-*d*$_6$, 90ºC) δ (ppm): 166.5, 163.4, 162.6, 159.4 (C1, C2, C4, C7), 140.0 (C5), 136.3, 135.6, 135.2 (C10, C15, C18), 128.3, 127.9, 127.9 (C11, C12, C13), 116.3, 115.4, 115.2 (C8, C16, C19), 97.7 (C6), 88.3 (C3), 67.8 (C9), 43.3 (C14), 43.0 (C17).

Positive ESI–MS: Expected mass for m/z, 372.5. Observed, 373.6 [(M+H$^+$)/z].

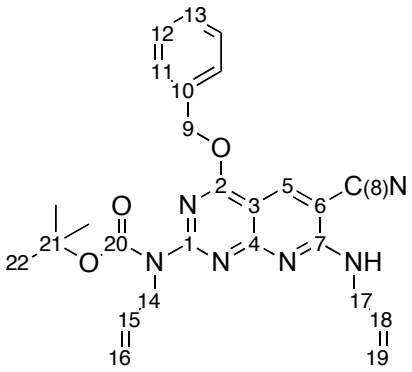

**Synthesis of compound 6.** Compound **5** (50 mg, 0.10 mmol) was dissolved in anhydrous DCM (5 mL) at rt under $N_2$ atmosphere. To this solution was added anhydrous $Et_3N$ (57 μL, 0.40 mmol) and DMAP (10 mg, 0.10 mmol) in anhydrous DCM (1 mL). The mixture was stirred at rt for 10 min, after which $Boc_2O$ (30 mg, 0.15 mmol) in anhydrous DCM (1 mL) was added. The reaction mixture was stirred at rt for 24 h and quenched with $dH_2O$ (10 mL). The DCM phase was washed with 10% aqueous citric acid, $dH_2O$, 5% aqueous $NaHCO_3$ and brine.

Pure compound **6** was obtained as a solid ($C_{26}H_{28}N_6O_3$, 31 mg, 50%) after silica gel column chromatography (0–100% EtOAc/Hexane). $R_f$ = 0.5 (30% EtOAc/Hexane). mp = 138–140ºC.

$^1$H–NMR (500 MHz, DMSO-*d*$_6$) δ (ppm): 8.61 (C5H, sharp s, 1H), 8.04 (NH, s, 1H), 7.52–7.34 (C11–13H, m, 5H), 5.98–5.85 (C15H and C18H, m, 2H), 5.55 (C9H, s, 2H), 5.17–5.05 (C16H and C19H, m, 4H), 4.48–4.47 (C14H, m, 2H), 4.10–4.08 (C17H, m, 2H), 1.45 (C22H, s, 9H).

$^{13}$C–NMR (125 MHz, DMSO-*d*$_6$) δ (ppm): 166.4, 162.1, 160.8, 159.0 (C1, C2, C4, C7), 152.8 (C20), 141.2 (C5), 135.8, 134.6, 134.2 (C10, C15, C18), 128.4, 128.2, 128.0 (C11, C12, C13), 116.0, 115.6, 115.5 (C8, C16, C19), 99.2 (C6), 93.3 (C3), 81.2 (C21), 68.4 (C9), 49.2 (C14), 43.0 (C17), 27.7 (C22).

Positive ESI–MS: Expected mass for m/z, 472.5. Observed, 473.6 [(M+H$^+$)/z].

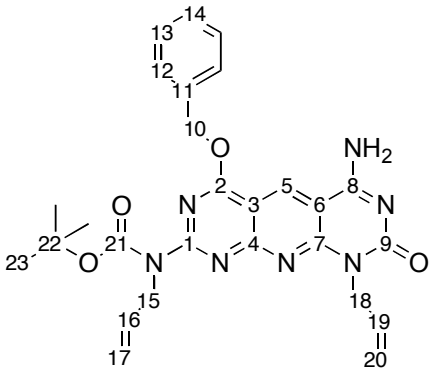


**Synthesis of compound 7.** To a solution of compound **6** (0.7 g, 1.55 mmol) in anhydrous DCM (15 mL) was added trichloroacetyl isocyanate (0.42 mL, 3.4 mmol) under $N_2$ atmosphere at 0ºC. The solution was stirred at 0ºC for 1 h and rt for 5 h. $NH_3$ in MeOH (7 M, 10 mL) was added to the reaction mixture and stirred for 16 h. The solvent was evaporated (rotovap) and the residue was purified by silica gel flash chromatography (0–100% EtOAc/Hexane) to yield compound **7** as a white powder ($C_{27}H_{29}N_7O_4$, 0.77 g, 90%). $R_f$ = 0.3 (100% EtOAc). mp = 208–209ºC.

$^1$H–NMR (500 MHz, $CD_2Cl_2$) δ (ppm): 8.93 (C5H, sharp s, 1H), 7.45–7.29 (C12–14H, m, 5H), 5.99–5.96 (C16H and C19H, m, 2H), 5.57 (C10H, s, 2H), 5.23–5.05 (C17H and C20H, m, 4H), 4.93 (C15, m, 2H), 4.65 (C18, m, 2H), 1.56 (C23H, s, 9H).

$^{13}$C–NMR (125 MHz, $CD_2Cl_2$) δ (ppm): 168.4, 162.9, 162.4, 162.0, 156.5, 156.0, 153.2 (C1, C2, C4, C7, C8, C9, C21), 135.8, 134.5, 133.1 (C5, C11, C16, C19), 129.0, 128.9, 128.8 (C12, C13,

C14), 116.5, 116.4 (C17, C20), 105.0, 104.1 (C3, C6), 82.6 (C22), 70.0 (C10), 50.2 (C15), 44.4 (C18), 28.2 (C23) .

Positive ESI–MS: Expected mass for m/z, 515.6. Observed, 516.5 [$(M+H^+)/z$].

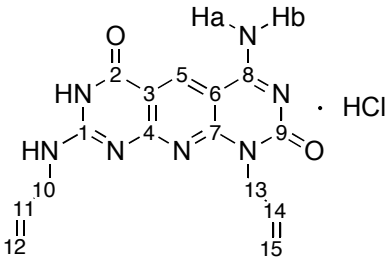


**Synthesis of ×G∧C.** A solution of compound **7** (0.4 g, 0.77 mmol) in HCl/dioxane (4 M, 30 mL) was heated at 90ºC for 6 h in a sealed tube. The solvent was evaporated (rotovap) and the residue was washed with DCM (3 × 10 mL) to yield ×G∧C as a white solid ($C_{15}H_{15}N_7O_2$, 0.22 g, 90%).

$^1$H–NMR (500 MHz, DMSO-$d_6$) δ (ppm): 11.57 (C2NH, s, 1H), 10.12 (C8NHa, 1H), 9.28 (C5H, sharp s, 1H), 8.94 (C8NHb, s, 1H), 7.65 (C10NH, s, 1H), 5.94–5.87 (C11H and C14H, m, 2H), 5.26–5.08 (C12H and C15H, m, 4H), 4.78 (C10H, m, 2H), 4.07 (C13H, m, 2H).

$^{13}$C–NMR (125 MHz, DMSO-$d_6$) δ (ppm): 163.9, 160.2, 157.5, 155.5, 154.0, 147.3 (C1, C2, C4, C7, C8, C9), 137.5, 133.9, 132.0 (C5, C11, C14), 116.4, 116.1 (C12, C15), 109.5 (C3), 99.1 (C6), 43.6, 42.7 (C10, C13).

High–resolution Positive ESI–MS: Expected mass for $(M+H^+)/z$, 326.1360. Observed, 326.1359.

Elemental Analysis, calculated for [$C_{15}H_{15}N_7O_2$-HCl]: C 49.80, H 4.46, N 27.10, Cl 9.80. Found: C 49.51, H 4.61, N 26.87, Cl 9.74.

Based on the characterization data, ×G∧C was isolated as an HCl salt and was used as is in the self-assembly studies. Attempts to use the free base resulted in extensive aggregation that hindered the imaging of the RNTs. Because protonation of the G or C face would prevent H-bonding and subsequent RNT self-assembly, we postulate that the protonation site is likely in the central pyridinic ring (the most basic).

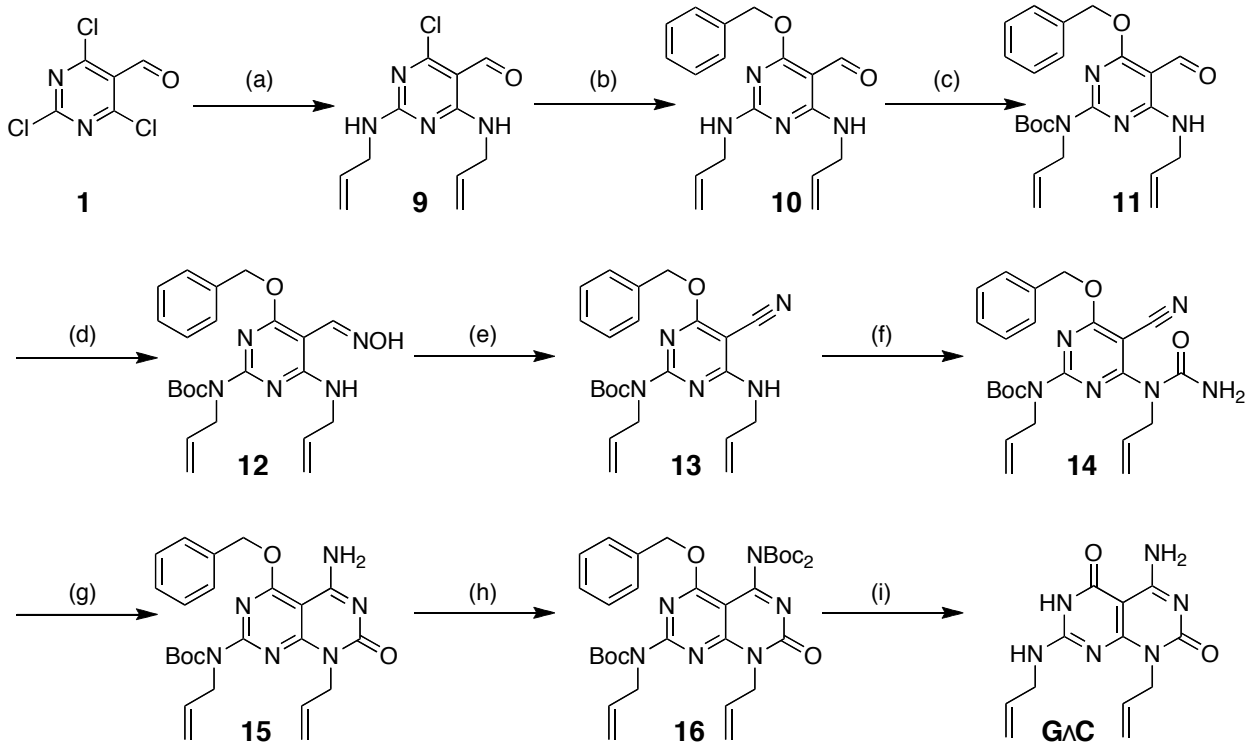


**Scheme S1.** Synthesis of **G∧C**: (a) allylamine, DCM, 2 h, 0ºC, 57%; (b) benzyl alcohol, NaH, THF, 16 h, reflux, 78%; (c) $(Boc)_2O$, $Et_3N$, THF, 6 h, 80%; (d) $NH_2OH$-HCl, pyridine, THF, 16 h, reflux, 80%; (e) TFAA, $Et_3N$, THF, 16 h, reflux, 84%; (f) N–chlorocarbonyl isocyanate, $Et_3N$, DCM, 2 h, 55%; (g) 7N $NH_3$ in MeOH, 2 h, 87%; (h) $(Boc)_2O$, $Et_3N$, THF, 16h, 83%; (i) 4M HCl in 1,4–dioxane, 6 h, 90ºC, 92%.

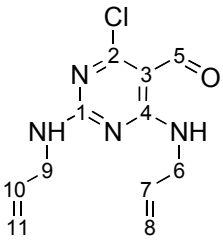

**Synthesis of Compound 9.** A solution of compound **1**[1] (1.0 g, 4.9 mmol) in DCM (10 mL) under $N_2$ atmosphere was cooled to 0ºC. Allylamine (1.13 mL, 14.6 mmol) was slowly added to this solution, followed by DIEA (1.35 mL, 14.6 mmol). The reaction mixture was stirred at rt for 4 h, after which the reaction was quenched with $dH_2O$ (10 mL). The organic layer was washed with $dH_2O$ and brine, dried over $Na_2SO_4$ and the solvent was evaporated (rotovap). Compound **9** ($C_{11}H_{13}ClN_4O$, 0.71 g, 57%) was obtained as a white solid after silica gel flash chromatography (5% EtOAc/hexane). $R_f$ = 0.26 (10% EtOAc/hexane). mp = 112–113°C.

$^1$H–NMR (500 MHz, $CDCl_3$) δ (ppm): Due to hydrogen bonding between C5O and C6NH,[2] two sets of peaks corresponding to a major and a minor species were observed in the $^1$H–NMR spectrum: 10.06, 10.04 (minor/major, C5H, s, 1H), 9.36, 9.17 (major/minor, C6NH, br s, 1H), 5.92–5.85 (C7H and C10H, m, 2H), 5.59, 5.39 (major/minor, C9NH, br s, 1H), 5.24–5.14 (C8H and C11H, m, 4H), 4.14–4.03 (C6H and C9H, m, 4H).

$^{13}$C–NMR (125 MHz, $CDCl_3$) δ (ppm): 188.7 (C5), 166.0, 162.5, 161.0 (C1, C2, C4), 134.0, 133.8 (C7, C10), 116.7 (C8, C11), 102.2 (C3), 44.1, 43.2 (C6, C9).

Positive ESI–MS: Expected mass for m/z, 252.1. Observed, 253.3 [$(M+H^+)/z$].

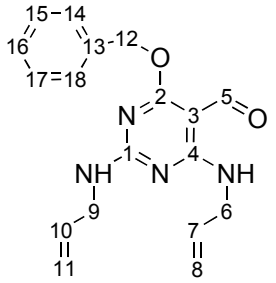


**Synthesis of compound 10.** To a solution of benzyl alcohol (0.25 mL, 2.5 mmol) in THF (15 mL) at rt under $N_2$ atmosphere was added NaH (0.20 g, 8.4 mmol). Compound **9** (0.70 g, 2.8 mmol) was then added and the reaction was heated to reflux and stirred for 16 h. The reaction mixture was cooled to 0ºC and quenched with saturated aqueous $NH_4Cl$ (5.0 mL). THF was evaporated (rotovap) and the residue was dissolved in diethyl ether, washed with $dH_2O$ and brine, dried over $Na_2SO_4$, and the solvent was evaporated (rotovap). The desired compound **10** ($C_{18}H_{20}N_4O_2$, 0.71 g, 78%) was obtained as a pale yellow oil after silica gel flash chromatography (5% EtOAc/hexane). $R_f$ = 0.26 (10% EtOAc/hexane).

$^1$H–NMR (400 MHz, $CDCl_3$) δ (ppm): Due to hydrogen bonding between C5O and C6NH,[2] two sets of peaks corresponding to a major and a minor species were observed in the $^1$H–NMR spectrum: 9.98 (C5H, s, 1H), 9.32, 9.18 (major/minor, C6NH, br s, 1H), 7.39–7.28 (C14H–C18H, m, 5H), 5.91–5.87 (C7, C10, m, 2H), 5.42–5.09 (C8H, C11H, C9NH, C12H, m, 7H), 4.13–4.04 (C6H, C9H, m, 4H).

$^{13}$C–NMR (100 MHz, $CDCl_3$) δ (ppm): Due to hydrogen bonding between C5O and C6NH, two sets of peaks corresponding to a major and a minor species were observed in the $^1$H–NMR

spectrum: 186.0 (C5), 172.0, 171.6 (C2), 163.4, 163.2 (C4), 162.7, 162.2 (C1), 136.6 (C13), 134.7, 134.5 (C7, C10), 128.5, 128.0, 127.7 (C14–C18), 116.3, 116.2, 115.9, 115.8 (C8, C11), 93.2, 93.0 (C3), 67.7, 67.5 (C12), 43.9 42.8, 42.6 (C6, C9).

Positive ESI–MS: Expected mass for m/z, 324.2. Observed, 325.4 [$(M+H^+)/z$].

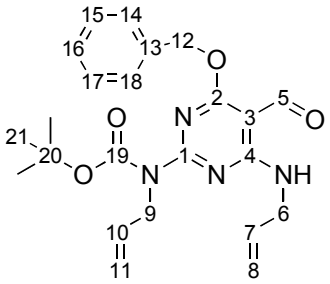


**Synthesis of compound 11.** To a solution of compound **10** (0.71 g, 2.2 mmol) in THF (15 mL) at rt under $N_2$ atmosphere was added DMAP (0.13 g, 1.1 mmol) and $Et_3N$ (1.2 mL, 8.7 mmol). $Boc_2O$ (0.71 g, 3.3 mmol) was quickly added and the reaction was stirred for 24 h. The reaction was quenched with $dH_2O$ (1 mL) and the THF was evaporated (rotovap). The residual solid was dissolved in EtOAc and washed with $dH_2O$, 10% citric acid, 5% $NaHCO_3$, and brine, dried over $Na_2SO_4$, and the solvent was evaporated (rotovap). Compound **11** ($C_{23}H_{28}N_4O_4$, 746 mg, 80%) was obtained as a colorless liquid after flash chromatography (2.5% EtOAc/hexane). $R_f$ = 0.77 (30% EtOAc/hexane).

$^1$H–NMR (500 MHz, $CDCl_3$) δ (ppm): 10.12 (C5H, s, 1H), 9.19 (C6NH, br s, 1H), 7.41–7.31 (C14H–C18H, m, 5H), 5.96–5.86 (C7H, C10H, m, 2H), 5.45 (C12H, s, 2H), 5.22–5.08 (C8H, C11H, m, 4H), 4.49 (C9H, app dt, *J* = 1.5 Hz, 5.5 Hz, 2H), 4.14 (C6H, app tt, *J* = 1.5 Hz, 5.5 Hz, 2H), 1.52 (C21H, s, 9H).

$^{13}$C–NMR (125 MHz, $CDCl_3$) δ (ppm): 187.3 (C5), 171.1 (C2), 162.7, 161.3 (C4, C1), 153.0 (C19), 136.3 (C13), 134.1, 134.0 (C7, C10), 128.4, 128.1, 128.0 (C14–C18), 116.3, 116.1 (C8, C11), 94.3 (C3), 81.8 (C20), 68.2 (C12), 49.6 (C9), 43.0 (C6), 28.1 (C21).

Positive ESI–MS: Expected mass for m/z, 424.2. Observed, 425.6 [$(M+H^+)/z$].

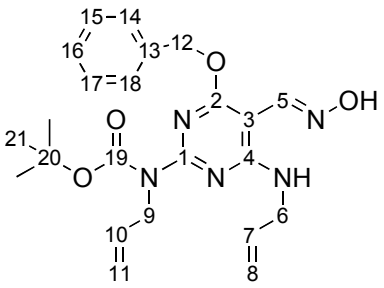

**Synthesis of Compound 12.** To a solution of compound **11** (0.74 g, 1.7 mmol) in THF (20 mL) and pyridine (0.35 mL) at rt under $N_2$ atmosphere was added hydroxylamine hydrochloride (0.24 g, 3.5 mmol). The reaction was heated to reflux for 16 h under $N_2$ atmosphere then cooled to rt and quenched with $dH_2O$ (5 mL). THF was evaporated under reduced pressure (rotovap) and the residual solid was dissolved in EtOAc, washed with $dH_2O$ and brine, dried over $Na_2SO_4$, and the solvent was evaporated (rotovap). Compound **12** ($C_{23}H_{29}N_5O_4$, 0.61 g, 80%) was obtained as a colorless oil after silica gel flash chromatography (0–10% EtOAc/hexane). $R_f$ = 0.54 (30% EtOAc/hexane).

$^1$H–NMR (500 MHz, $CDCl_3$) δ (ppm): 8.52 (C5H, s, 1H), 7.95 (C6NH, br t, $J$ = 5 Hz, 1H), 7.40–7.30 (C14H–C18H, m, 5H), 5.96–5.89 (C7H, C10H, m, 2H), 5.38 (C12H, s, 2H), 5.21–5.05 (C8H, C11H, m, 4H), 4.45 (C9H, app dt, $J$ = 1.5 Hz, 5 Hz, 2H) 4.16 (C6H, app tt, $J$ = 1.5 Hz, 5.5 Hz, 2H), 1.50 (C21H, s, 9H).

$^{13}$C–NMR (125 MHz, $CDCl_3$) δ (ppm): 167.1 (C2), 160.7, 158.4 (C1, C4), 153.9 (C19), 145.7 (C5), 136.8 (C13), 134.8, 134.5 (C7, C10), 128.4, 127.9 127.8 (C14–C18), 116.1, 115.5 (C8, C11), 88.2 (C3), 81.5 (C20), 68.1 (C12), 49.9 (C9), 43.4 (C6), 28.3 (C21).

Positive ESI–MS: Expected mass for m/z, 439.2. Observed, 440.6 [$(M+H^+)$/z].

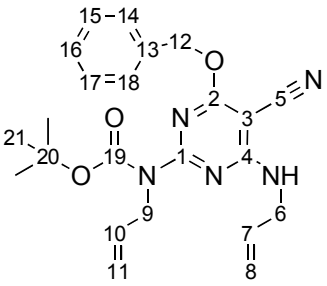

**Synthesis of compound 13.** A solution of compound **12** (0.61 g, 1.38 mmol) in THF (20 mL) at rt under $N_2$ atmosphere was treated with $Et_3N$ (0.60 mL, 4.16 mmol). The solution was cooled to 0ºC and TFAA (0.30 mL, 2.1 mmol) was slowly added. The reaction was stirred for 15 min at 0ºC, allowed to warm to rt, and then heated to reflux for 16 h. The solution was cooled to 0ºC and quenched with $dH_2O$ (1 mL). The THF was evaporated under reduced pressure (rotovap) and the residual solid was dissolved in EtOAc and

washed with $dH_2O$, 10% aqueous citric acid, 5% aqueous $NaHCO_3$, dried over $Na_2SO_4$, and the solvent was evaporated (rotovap). Compound **13** ($C_{23}H_{27}N_5O_3$, 0.49 g, 84%) was obtained as an amorphous solid after silica gel chromatography (0–10% EtOAc/hexane). $R_f$ = 0.71 (30% EtOAc/hexane).

$^1$H–NMR (500 MHz, $CDCl_3$) δ (ppm): 7.42–7.26 (C14H–C18H, m, 5H), 5.91–5.83 (C7H, C10H, m, 2H), 5.43 (C12H, s, 2H), 5.40 (C6NH, br t, *J* = 5.5 Hz, 1H), 5.24–5.07 (C8H, C11H, m, 4H), 4.45 (C9H, app dt, *J* = 1.5 Hz, 5.5 Hz, 2H), 4.12 (C6H, app tt, *J* = 1.5 Hz, 5.5 Hz, 2H), 1.51 (C21H, s, 9H).

$^{13}$C–NMR (125 MHz, $CDCl_3$) δ (ppm): 170.5 (C2), 164.2, 160.4 (C1, C4), 153.0 (C19), 136.0 (C13), 134.0, 133.9 (C7, C10), 128.5, 128.2, 128.0 (C14–C18) 117.0, 116.4 (C8, C11), 114.7 (C5), 82.1 (C20), 69.2 (C3), 68.6 (C12), 49.7 (C9), 43.7 (C6), 28.2 (C21).

Positive ESI–MS: Expected mass for m/z, 421.2. Observed, 422.6 [$(M+H^+)/z$].

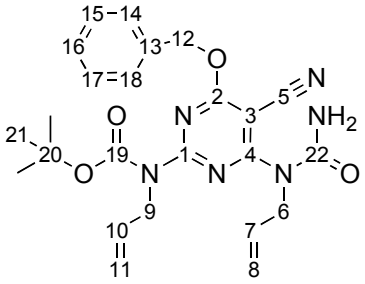


**Synthesis of Compound 14.** A solution of compound **13** (1.0 g, 2.37 mmol) in DCM (10 mL) at rt under $N_2$ atmosphere was treated with $Et_3N$ (1.32 mL, 9.48 mmol). The solution was cooled to 0ºC and *N*–chlorocarbonyl isocyanate (0.38 mL, 4.74 mmol) was slowly added. The reaction was allowed to warm to rt and stirred for 2 h. The reaction was quenched with $dH_2O$ (2 mL), the organic layer was separated and evaporated (rotovap). The desired compound **14** ($C_{24}H_{28}N_6O_4$, 605 mg, 55%) was isolated as a white solid after silica gel flash chromatography (25% EtOAc/hexane). $R_f$ = 0.54 (50% EtOAc /hexane). mp = 129–131°C.

$^1$H–NMR (500 MHz, $CDCl_3$) δ (ppm): 7.40–7.30 (C14H–C18H, m, 5H), 5.89–5.80 (C7H, C10H, m, 2H), 5.46 (C12H, s, 2H), 5.25–5.13 (C8H, C11H, m, 4H), 4.90 (C6H, app dt, *J* = 1.5 Hz, 5 Hz, 2H), 4.50 (C9H, app dt, *J* = 1.5 Hz, 5.5 Hz, 2H), 1.50 (C21H, s, 9H).

$^{13}$C–NMR (125 MHz, $CDCl_3$) δ (ppm): 171.9 (C2), 163.2, 158.2 (C1, C4), 155.3, 151.9 (C19, C22), 135.1 (C13), 133.3, 133.0 (C7, C10), 128.4, 128.2, 127.4 (C14 – C18), 116.7, 116.6 (C8, C11), 113.6 (C5), 83.2 (C20), 78.2 (C3), 69.5 (C12), 49.4 (C9), 48.1 (C6), 27.8 (C21).

Positive ESI–MS: Expected mass for m/z, 464.2. Observed, 465.6 [$(M+H^+)/z$].

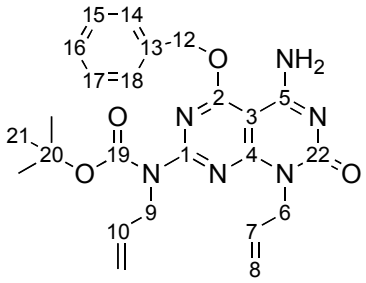

**Synthesis of compound 15.** Compound **14** (0.61g, 1.31 mmol) was stirred in 7M $NH_3$ in MeOH (30 mL) at rt for 2 h. The solvent was evaporated under reduced pressure (rotovap) and the residue was dissolved in DCM and washed with water. The organic layer was separated and concentrated (rotovap). The solid was triturated with ether to yield the desired product **15** ($C_{24}H_{28}N_6O_4$, 0.53 g, 87%) as a white solid. $R_f$ = 0.24 (5% MeOH/DCM). mp = 101–103°C.

$^1$H–NMR (500 MHz, $CDCl_3$) δ (ppm): 7.45–7.34 (C14H–C18H, m, 5H), 7.09 (C5NH, br s, 1H), 5.94–5.88 (C7H, C10H, m, 2H), 5.58 (C12H, s, 2H), 5.22–5.11 (C8H, C11H, m, 4H), 4.79 (C6H, d, *J* = 5.5 Hz, 2H), 4.55 (C9H, app dt, *J* = 1.5 Hz, 5.0 Hz, 2H), 1.53 (C21H, s, 9H).

$^{13}$C–NMR (125 MHz, $CDCl_3$) δ (ppm): 166.7 (C2), 161.3, 160.6, 160.4 (C1, C4, C5), 155.8, 152.6 (C19, C22), 135.2 (C13), 133.6, 132.6 (C7, C10), 128.9, 128.8, 128.6 (C14–C18), 117.4, 116.6 (C8, C11), 86.4 (C3), 82.6 (C20), 69.9 (C12), 49.9 (C9), 44.6 (C6), 28.2 (C21).

Positive ESI–MS: Expected mass for m/z, 464.2. Observed, 465.6 [$(M+H^+)/z$].

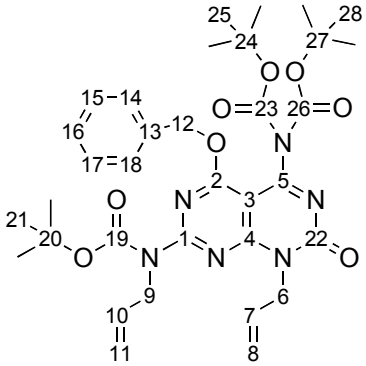

**Synthesis of compound 16.** A solution of compound **15** (8.27 g, 17.8 mmol) in THF (250 mL) at rt under $N_2$ atmosphere was treated with $Et_3N$ (15 mL, 107 mmol) and DMAP (2.17g, 17.8 mmol). $Boc_2O$ (11.7 g, 53.4 mmol) was added and the reaction was stirred for 16 h at rt. The THF was evaporated (rotovap) and

the residue was dissolved in EtOAc and washed with $dH_2O$, 10% aqueous citric acid, 5% aqueous $NaHCO_3$, and brine, dried over $Na_2SO_4$, and the solvent was evaporated (rotovap). The desired compound **16** ($C_{34}H_{44}N_6O_8$, 9.81 g, 83%) was isolated as a yellow oil after silica gel flash chromatography (10–20% EtOAc/hexane). $R_f$ = 0.51 (30% EtOAc/hexane).

$^1$H–NMR (600 MHz, $CDCl_3$) δ (ppm): 7.42–7.30 (C14H–C18H, m, 5H), 5.96–5.87 (C7H, C10H, m, 2H), 5.53 (C12H, s, 2H), 5.20–5.14 (C8H, C11H, m, 4H), 4.89 (C6H, d, *J* = 6.0 Hz, 2H), 4.54 (C9H, d, *J* = 5.4 Hz, 2H), 1.54 (C21H, s, 9H), 1.30 (C25H, C28H, s, 18H).

$^{13}$C–NMR (125 MHz, $CDCl_3$) δ (ppm): 165.6 (C2), 160.7, 160.6, 160.2 (C1, C4, C5), 155.1, 151.9 (C19, C22), 149.0 (C23, C26), 134.7 (C13), 133.0, 131.0 (C7, C10), 128.4, 128.2 (C14–C18), 117.8, 116.6 (C8, C11), 92.8 (C3), 83.5 (C24, C27), 82.9 (C20), 69.9 (C12), 49.7 (C9), 45.1 (C6), 27.8 (C21), 27.6 (C25, C28).

Positive ESI–MS: Expected mass for m/z, 664.3. Observed, 665.8 [(M+H$^+$)/z].

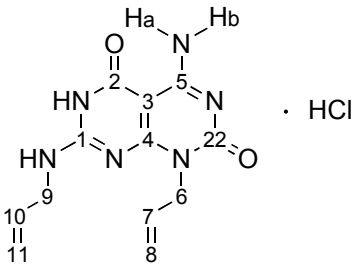

· HCl

**Synthesis of allyl-substituted G∧C.** A solution of compound **16** (0.42 g, 0.77 mmol) in 4M HCl/dioxane (30 mL) was heated at 90ºC for 6 h in a sealed tube. The solvent was then evaporated (rotovap) and the residue was washed with DCM three times to yield compound G∧C as a white solid ($C_{12}H_{14}N_6O_2$, 0.2 g, 92%).

$^1$H–NMR (600 MHz, DMSO-$d_6$) δ (ppm): 12.11 (C2NH, 1H), 9.08 (C5NHa, 1H), 8.44 (C5NHb, 1H), 8.23 (C9NH, 1H), 5.89–5.77 (C7H, C10H, m, 2H), 5.21–5.10 (C8H, C11H, m, 4H), 4.58–4.57 (C6H, m, 2H), 4.01–3.98 (C9H, m, 2H).

$^{13}$C–NMR (150 MHz, DMSO-$d_6$) δ (ppm): 161.2, 159.8, 156.2, 155.2 (C1, C2, C4, C5), 147.9 (C22), 133.7, 131.8 (C7, C10), 117.4, 116.5 (C8, C11), 82.6 (C3), 44.1, 43.1 (C6, C9).

High–resolution Positive ESI–MS: Expected mass for (M+H$^+$)/z, 275.1178. Observed, 275.1251.

Elemental analysis, calculated for [$C_{15}H_{15}N_7O_2$–HCl]: C46.38, H 4.87, N 27.05, Cl 11.41. Found: C 46.15, H 4.84, N 26.53, Cl 11.24.

# $^{1}H/^{13}C$ NMR Data

## Compound 2

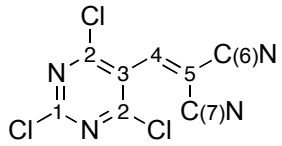


### $^{1}H$–NMR (600 MHz, $CDCl_3$)

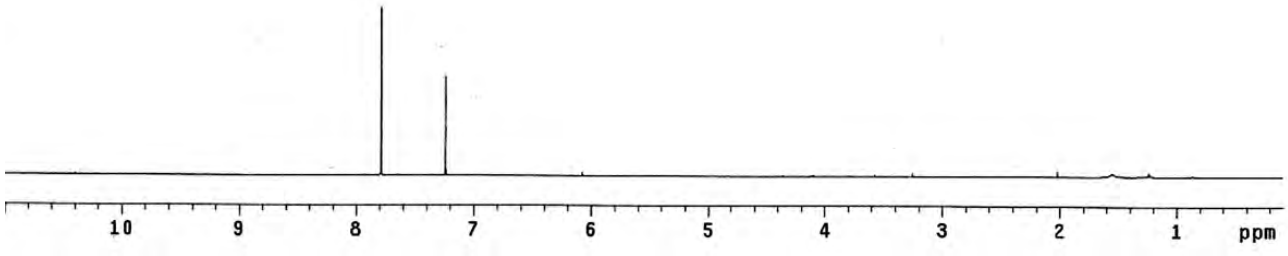


### $^{13}C$–NMR (150 MHz, $CDCl_3$)

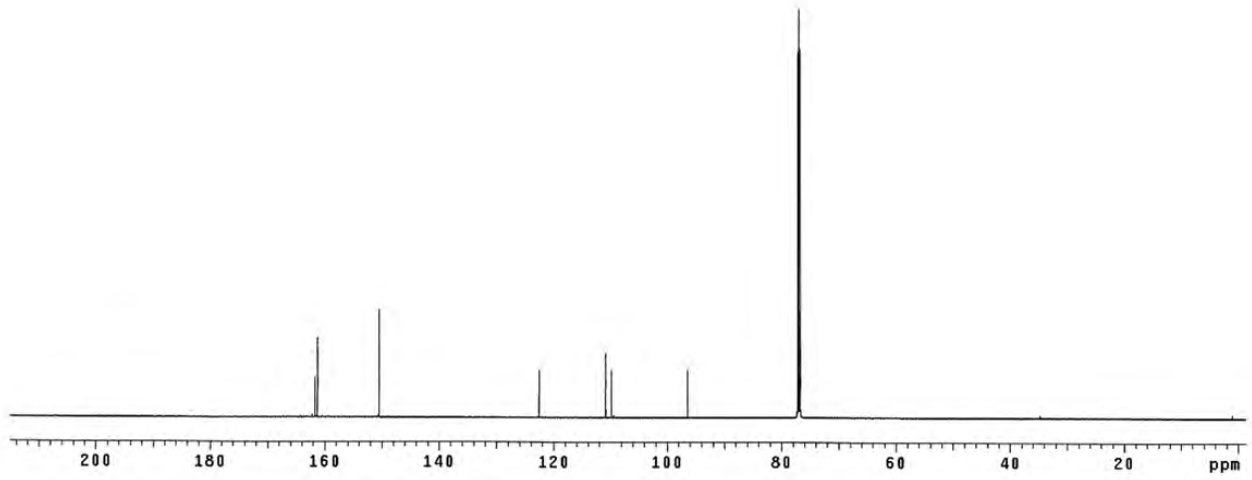

**Compound 3**

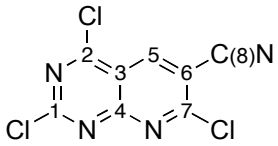


**$^{1}$H–NMR (500 MHz, $CDCl_3$)**

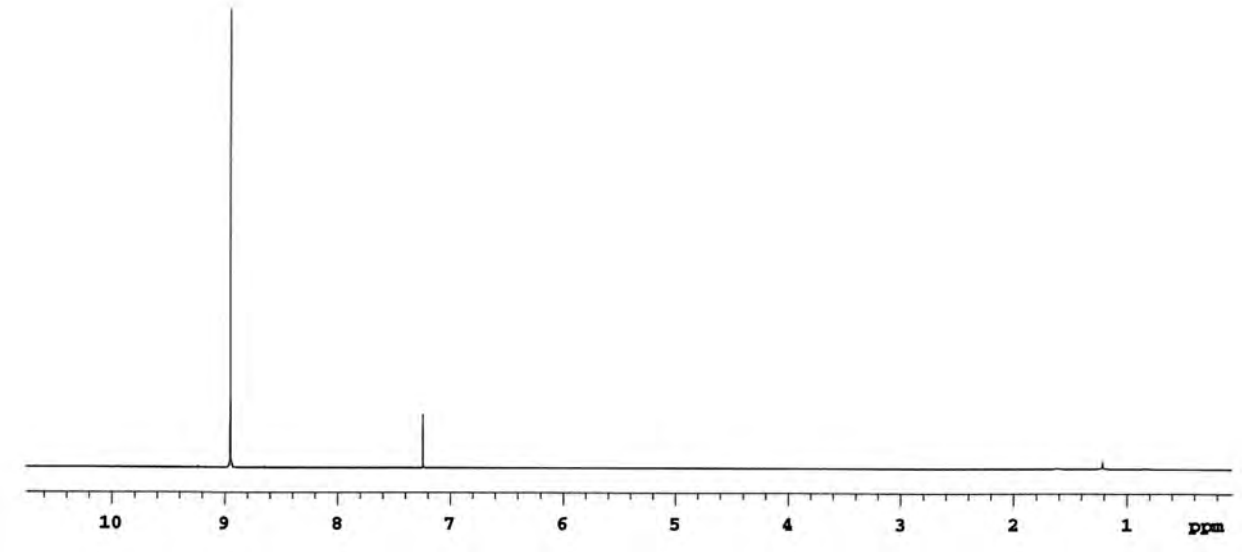


**$^{13}$C–NMR (125 MHz, $CDCl_3$)**

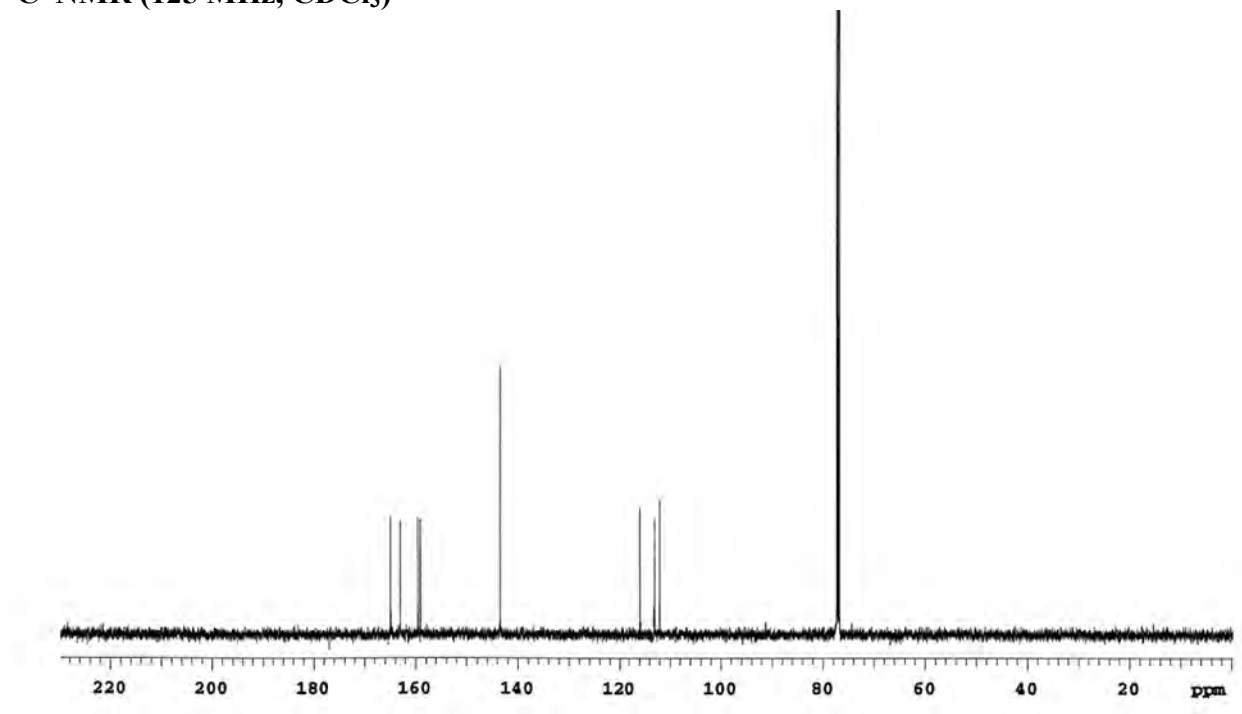

**Compound 4**

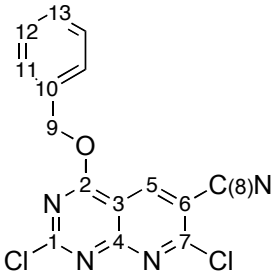


**$^{1}$H–NMR (600 MHz, $CDCl_3$)**

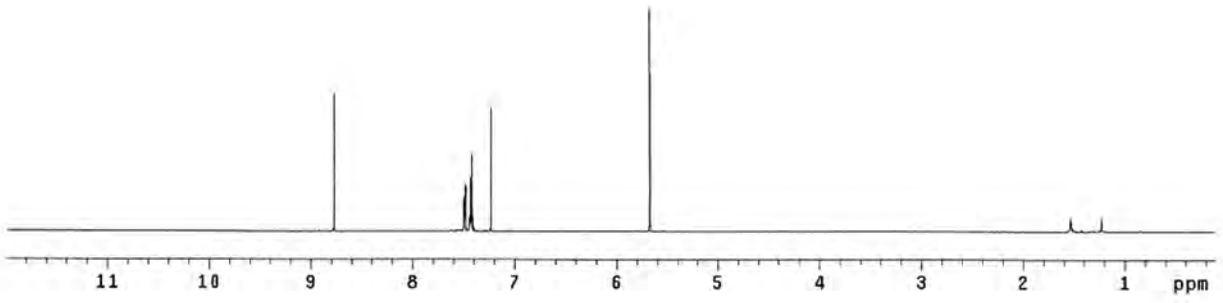


**$^{13}$C–NMR (150 MHz, $CDCl_3$)**

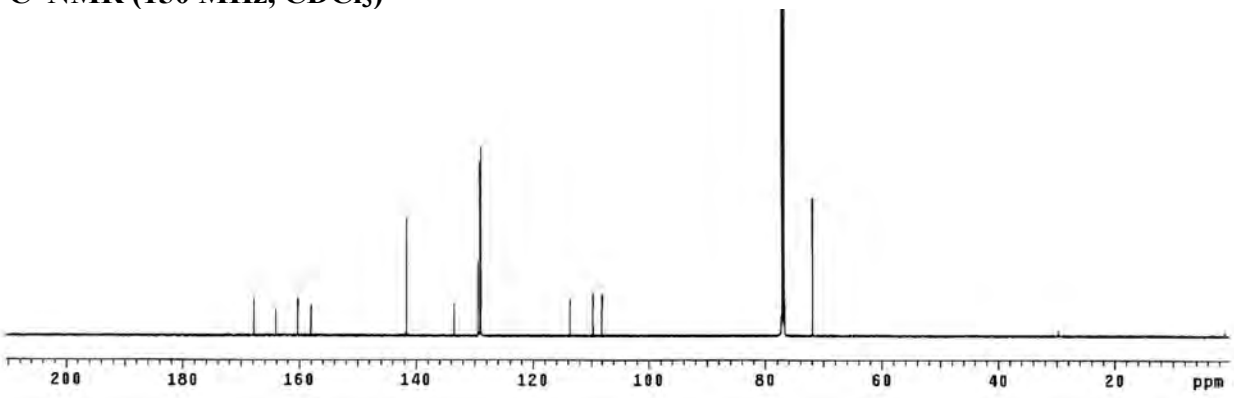

**Compound 5**

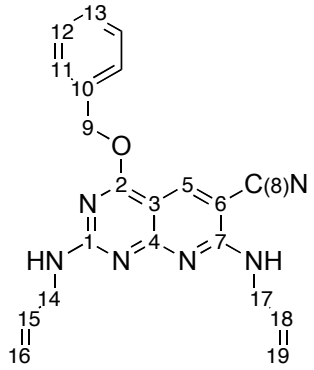


**$^{1}$H–NMR (500 MHz, DMSO-$d_6$, 90ºC)**

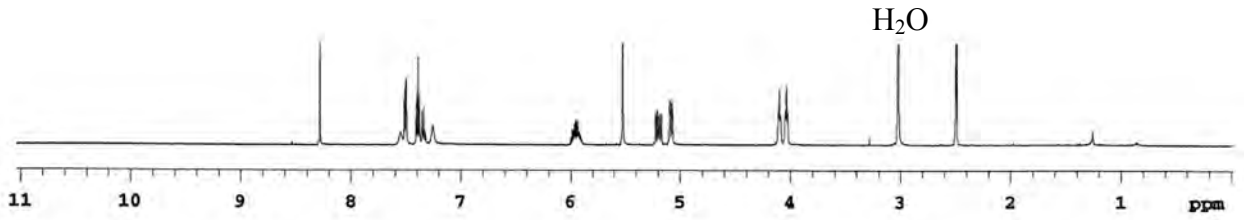


**$^{13}$C–NMR (125 MHz, DMSO-$d_6$, 90ºC)**

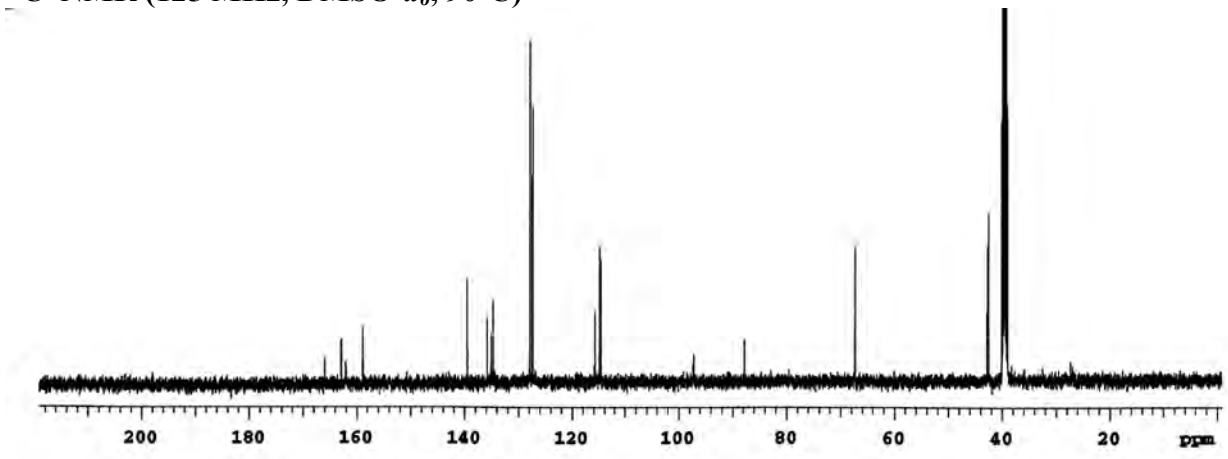

**Compound 6**

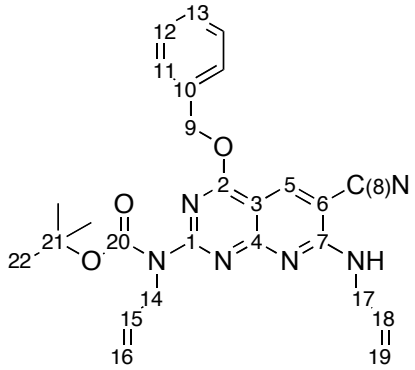


**$^{1}$H–NMR (500 MHz, DMSO-$d_6$)**

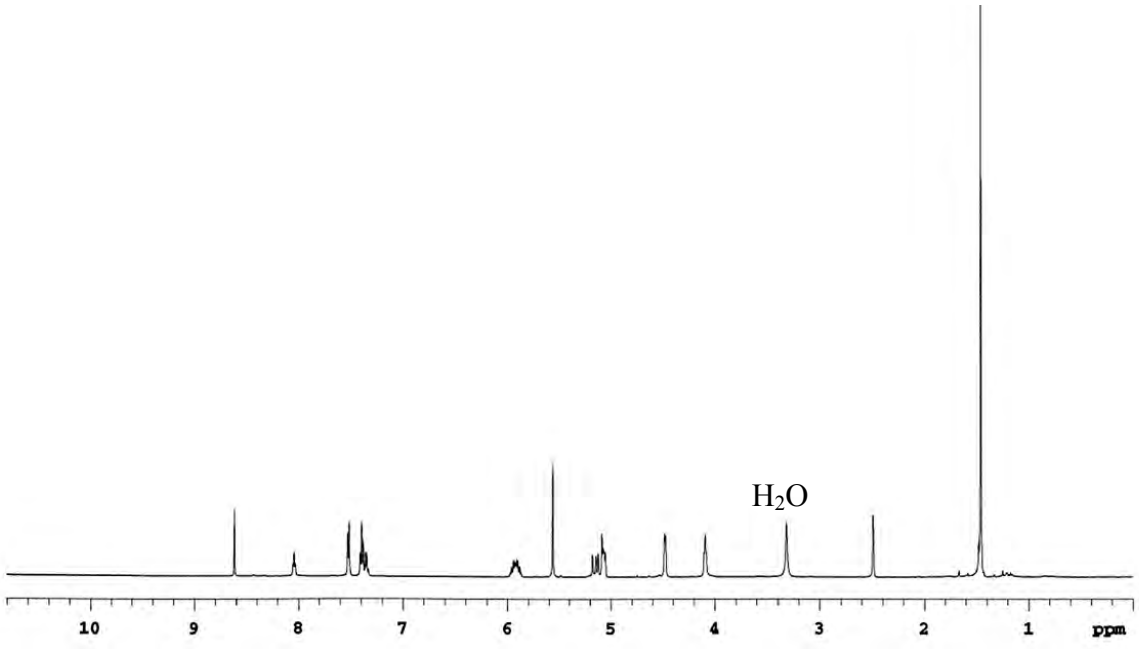


**$^{13}$C–NMR (125 MHz, DMSO-$d_6$)**

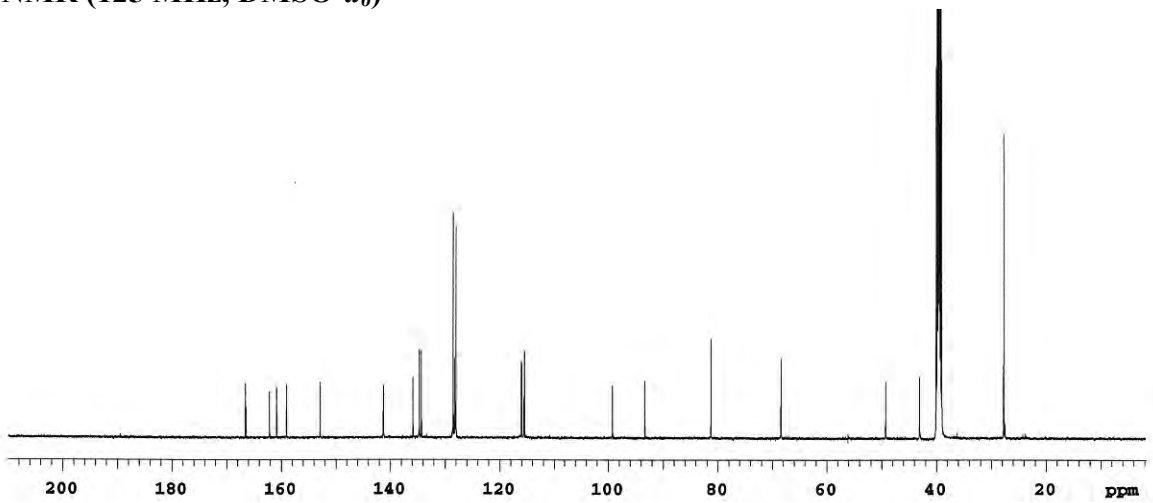

**Compound 7**

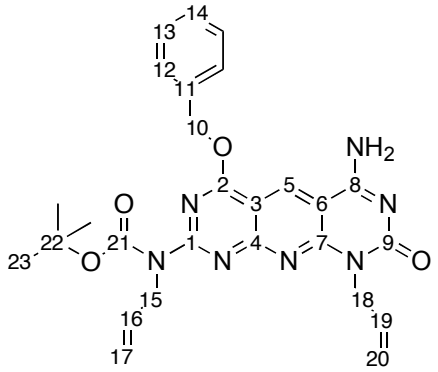


**$^{1}$H–NMR (500 MHz, $CD_2Cl_2$)**

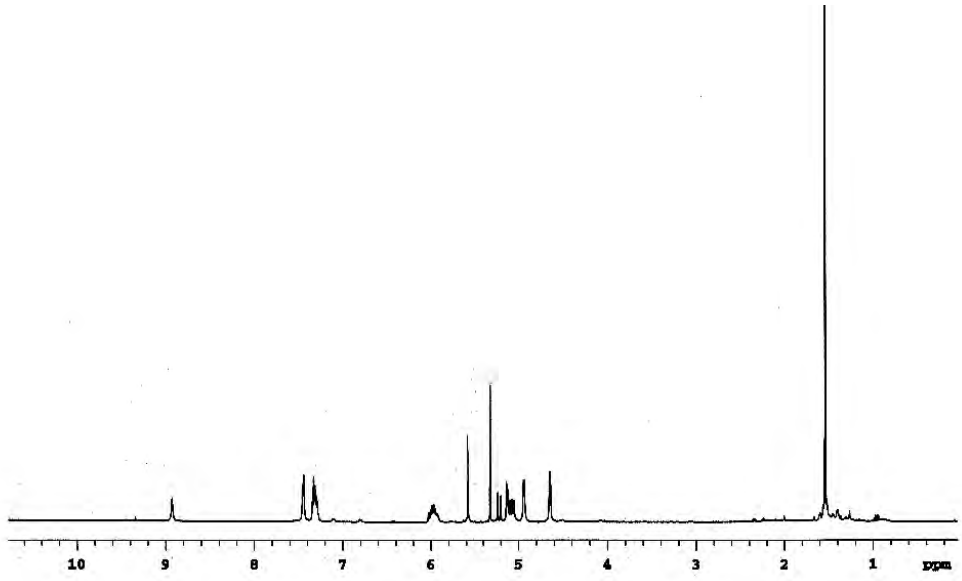


**$^{13}$C–NMR (125 MHz, $CD_2Cl_2$)**

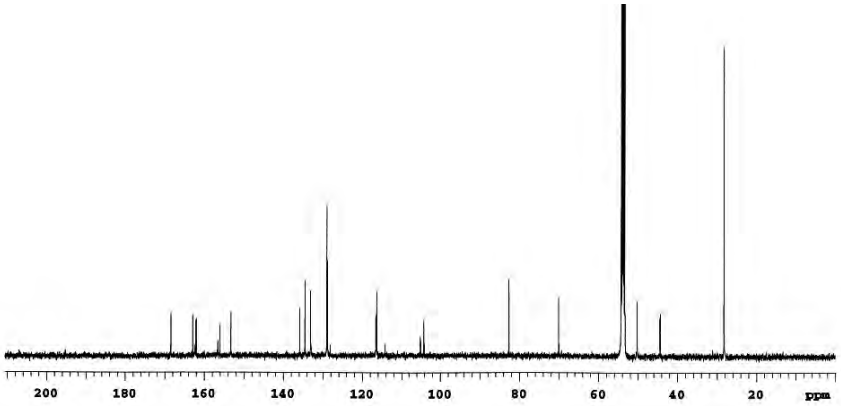

**×G∧C**

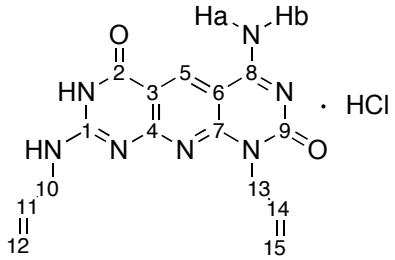


**$^{1}$H–NMR (500 MHz, DMSO-$d_6$)**

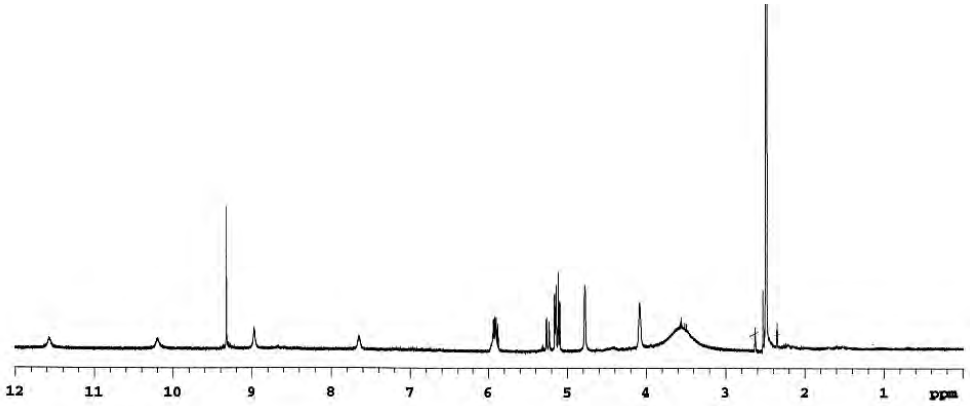


**$^{13}$C–NMR (125 MHz, DMSO-$d_6$)**

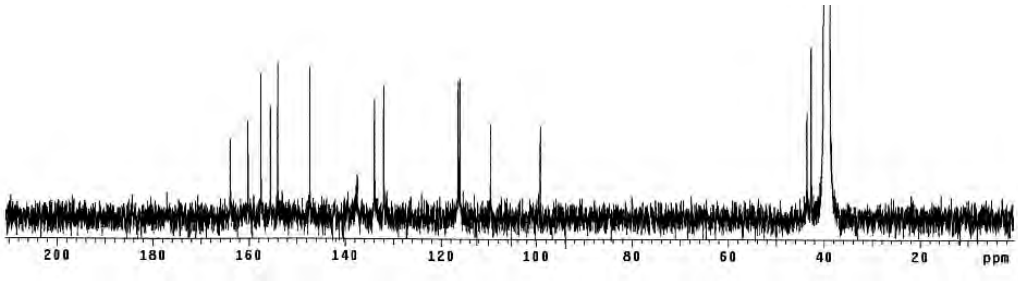

**Compound 9**

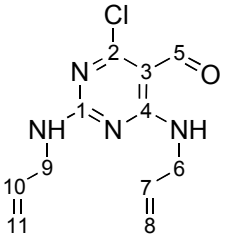


**$^{1}$H–NMR (500 MHz, $CDCl_3$)**

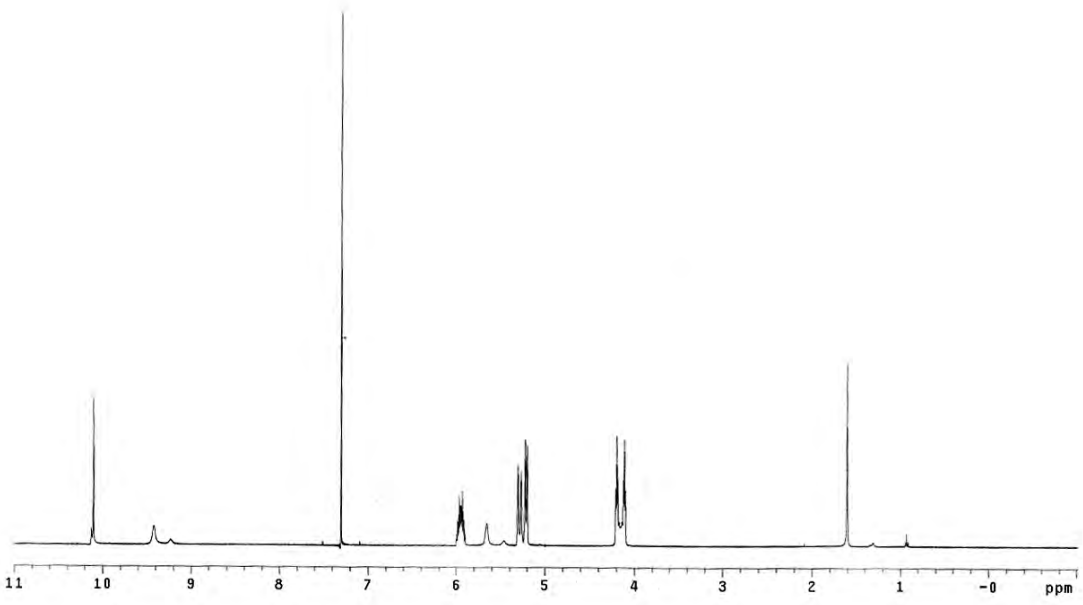


**$^{13}$C–NMR (125 MHz, $CDCl_3$)**

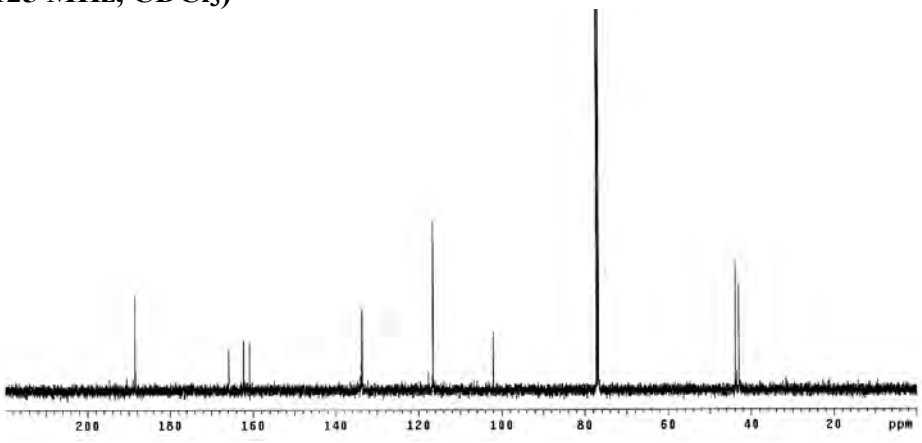

## Compound 10

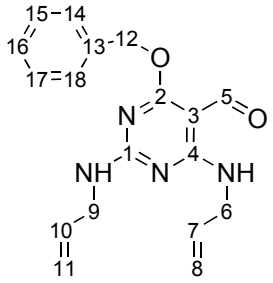


## $^{1}$H–NMR (400 MHz, $CDCl_3$)

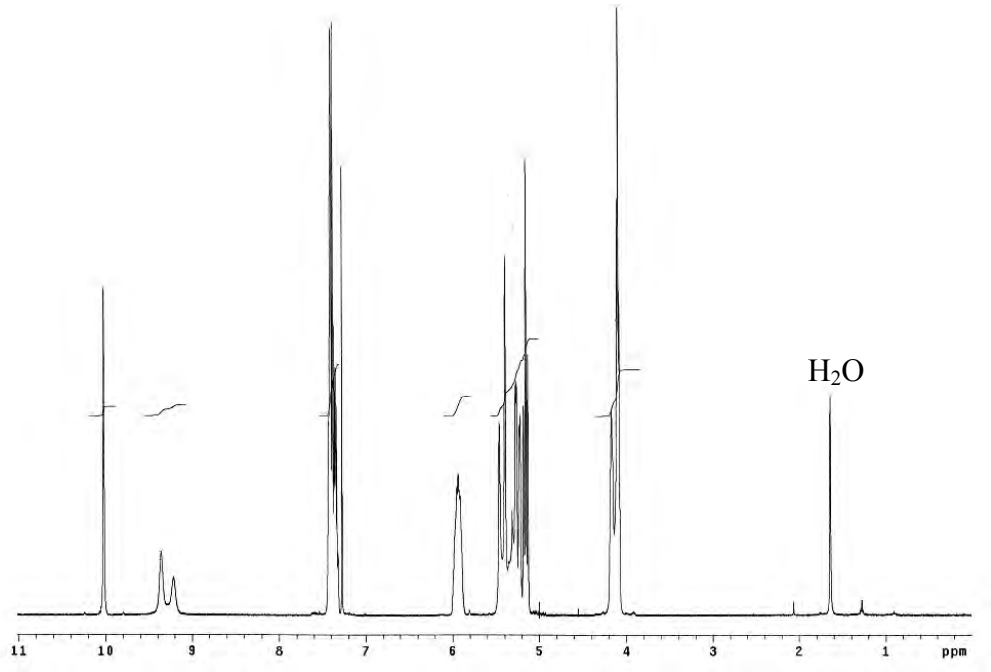


## $^{13}$C–NMR (100 MHz, $CDCl_3$)

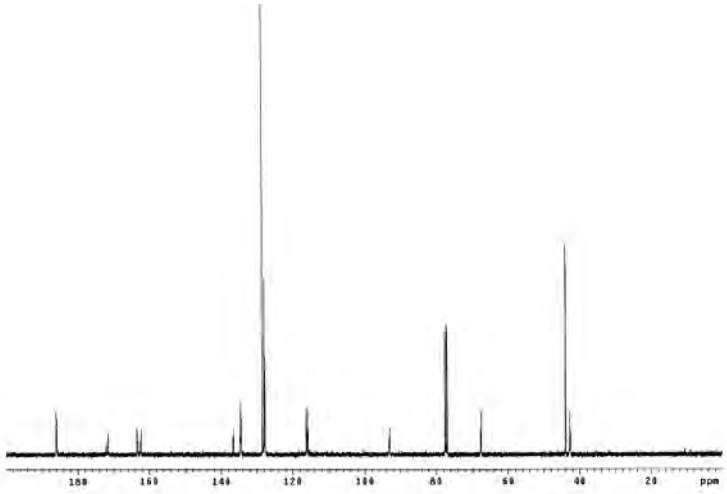

**Compound 11**

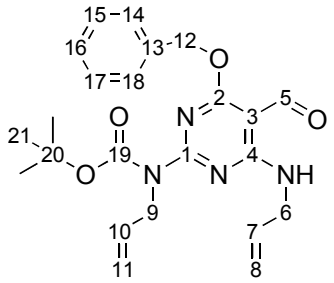


**$^{1}$H–NMR (500 MHz, $CDCl_3$)**

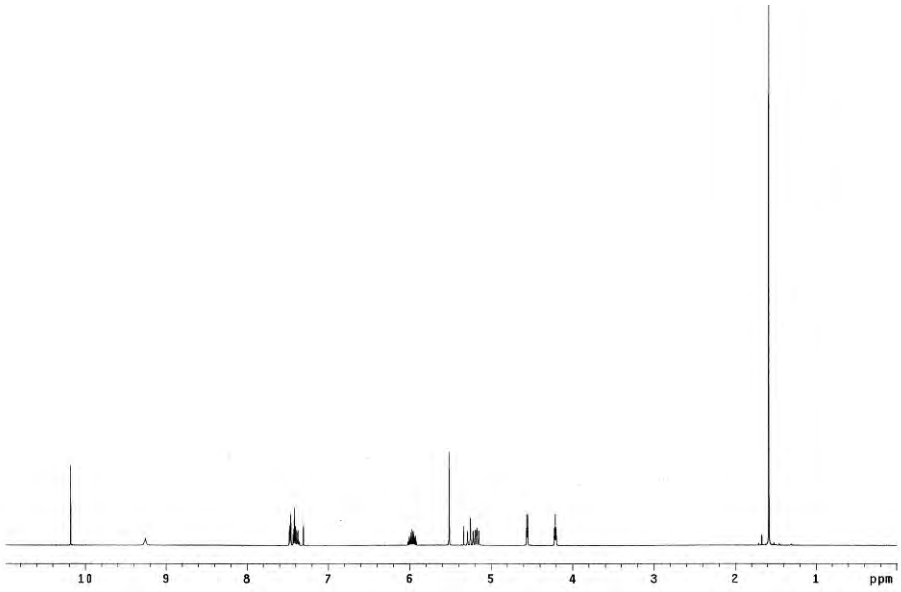


**$^{13}$C–NMR (125 MHz, $CDCl_3$)**

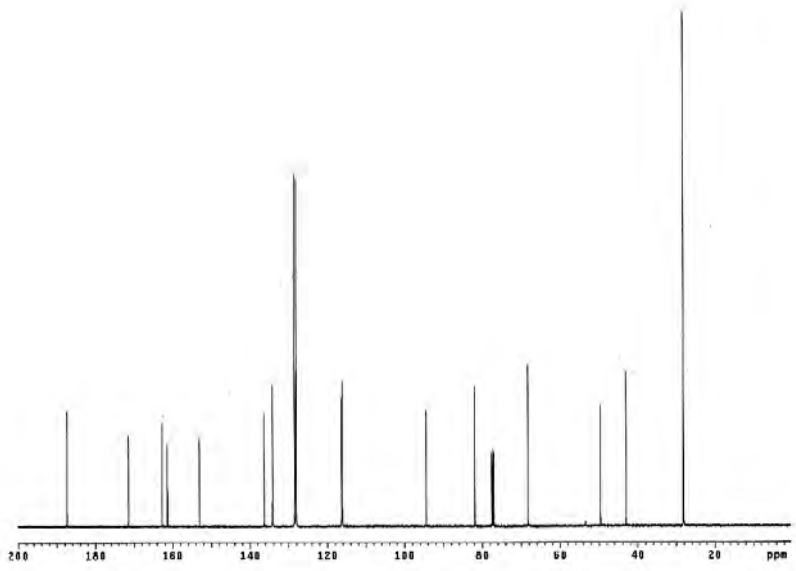

**Compound 12**

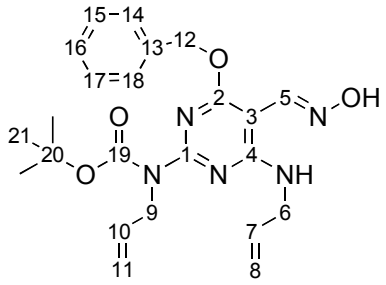


**$^{1}$H–NMR (500 MHz, $CDCl_3$)**

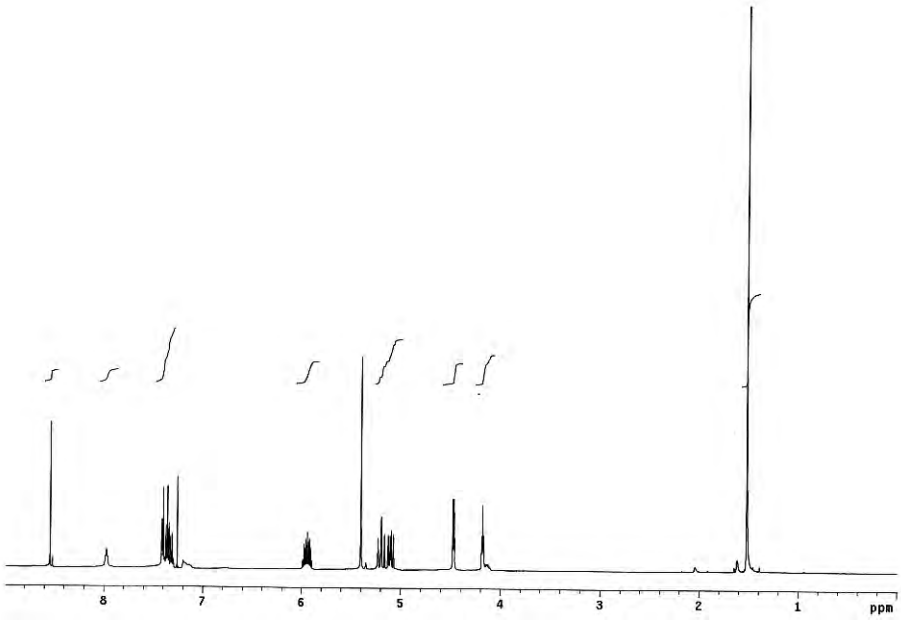


**$^{13}$C–NMR (125 MHz, $CDCl_3$)**

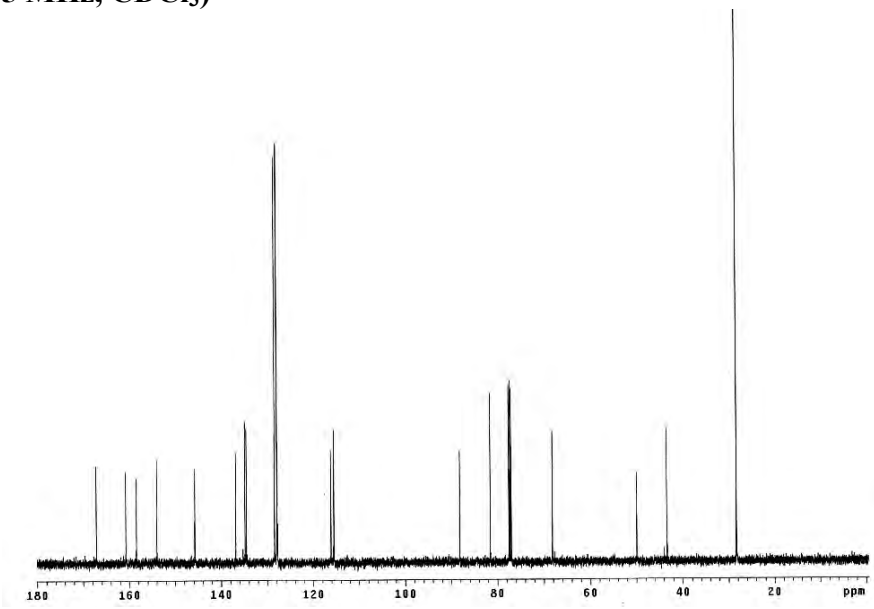

**Compound 13**

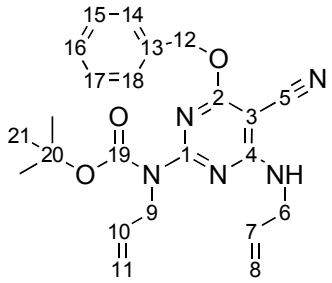


**$^{1}$H–NMR (500 MHz, $CDCl_3$)**

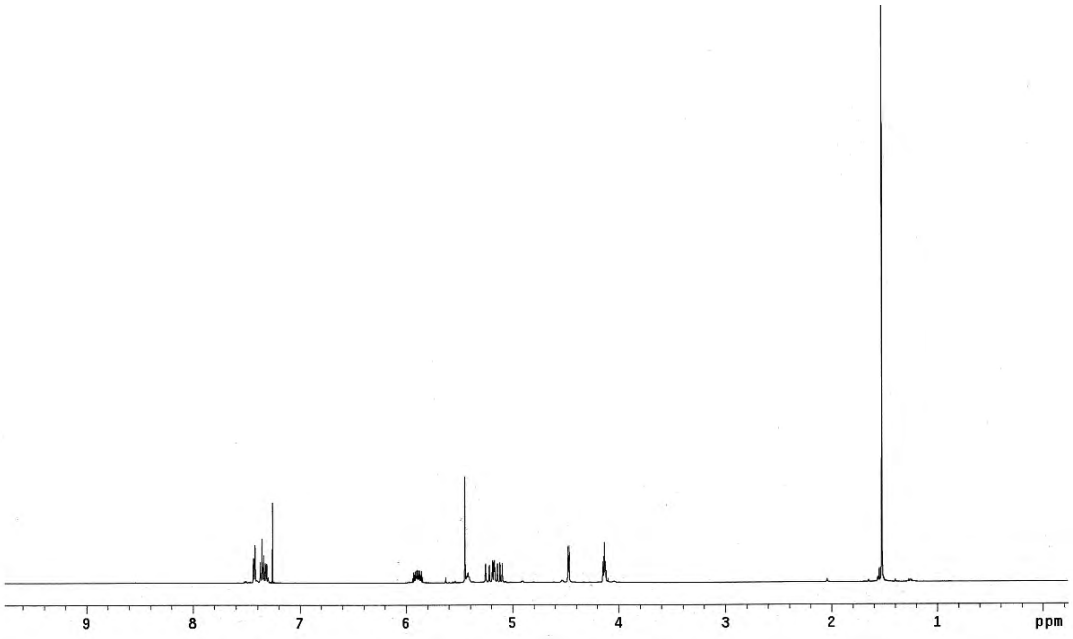


**$^{13}$C–NMR (125 MHz, $CDCl_3$)**

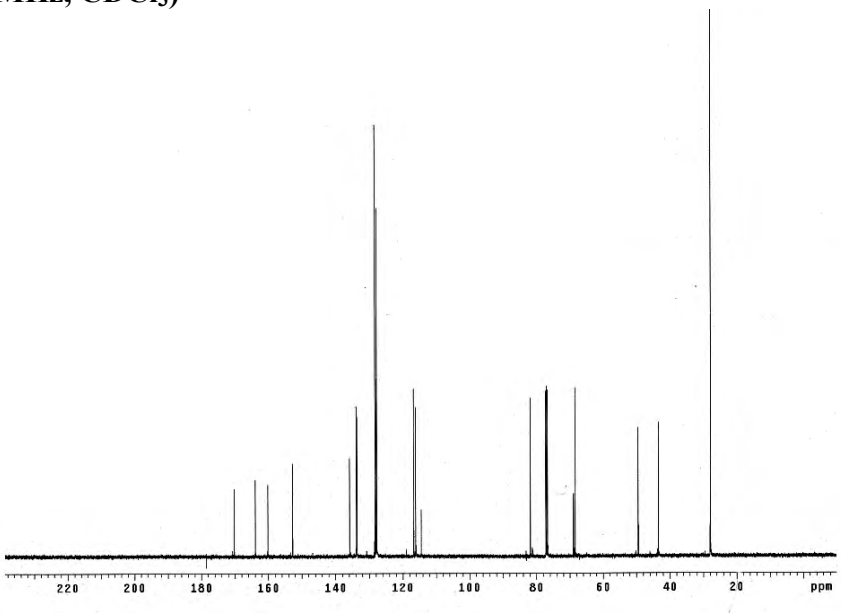

**Compound 14**

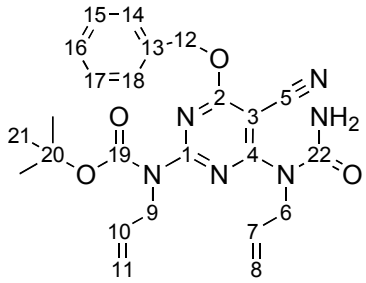


**$^{1}$H–NMR (500 MHz, $CDCl_3$)**

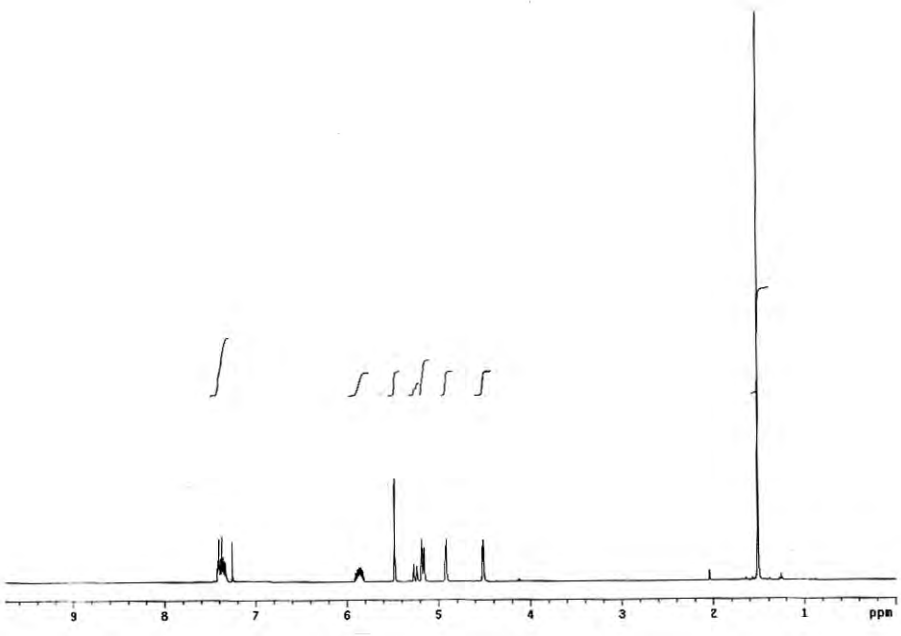


**$^{13}$C–NMR (125 MHz, $CDCl_3$)**

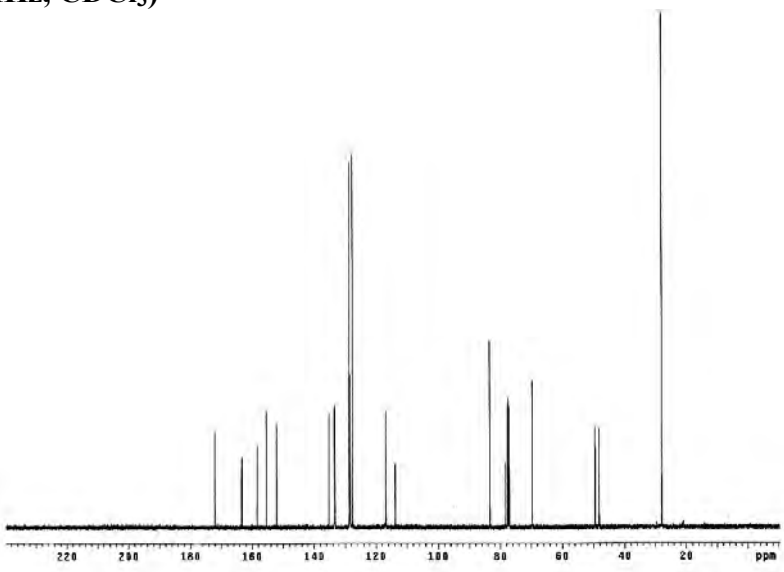

**Compound 15**

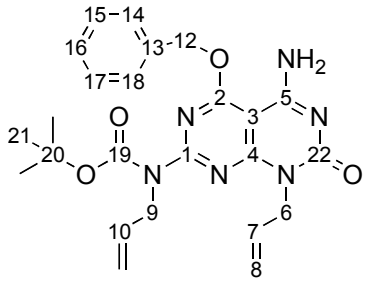


**$^{1}$H–NMR (500 MHz, $CDCl_3$)**

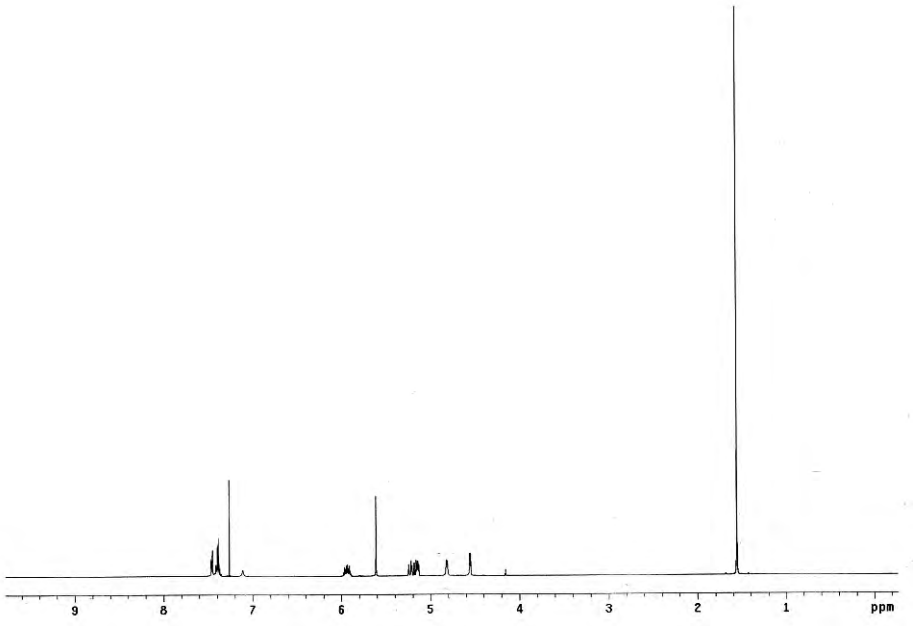


**$^{13}$C–NMR (125 MHz, $CDCl_3$)**

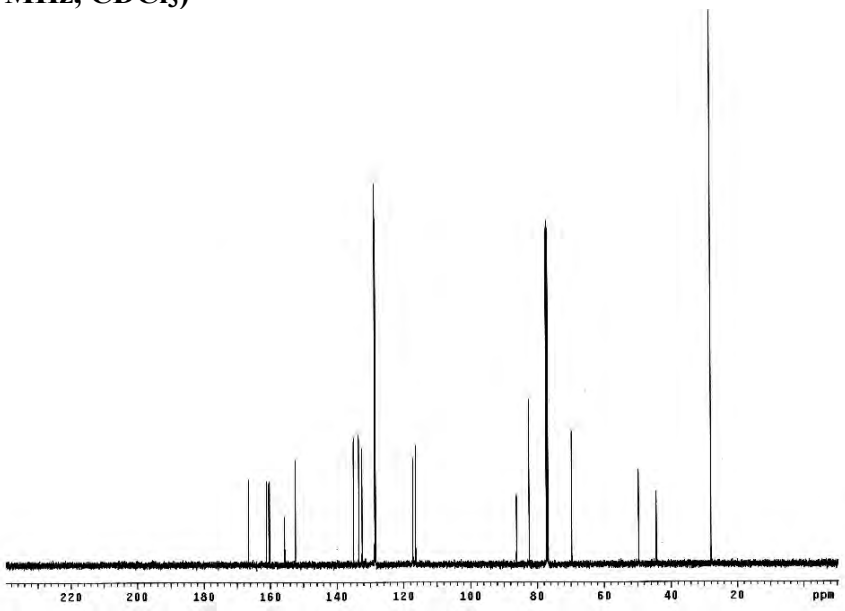

**Compound 16**

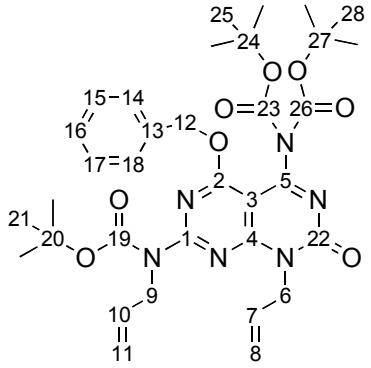


**$^{1}$H–NMR (600 MHz, $CDCl_3$)**

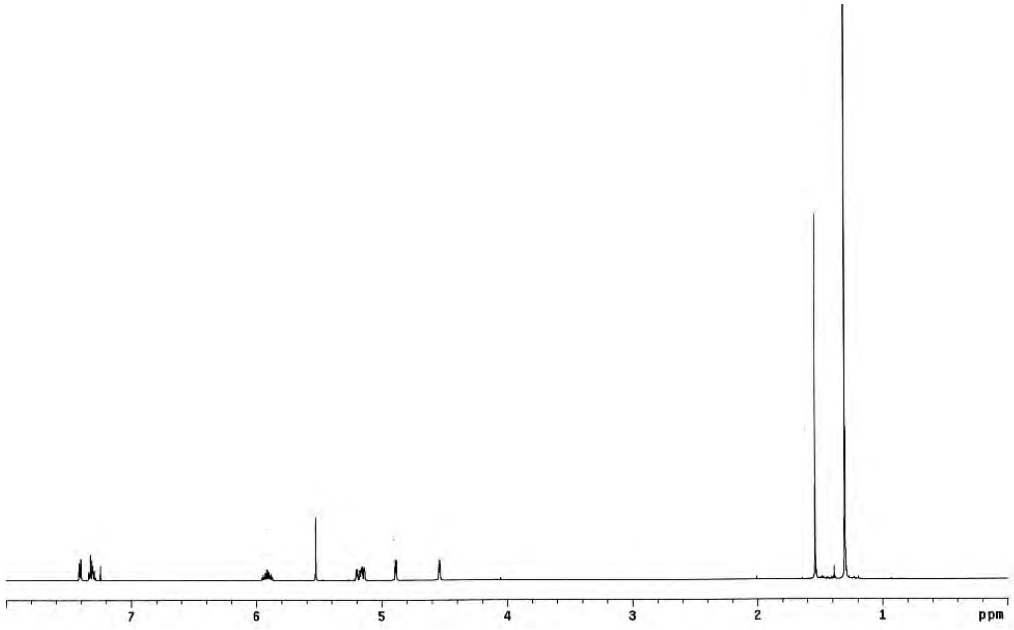


**$^{13}$C–NMR (125 MHz, $CDCl_3$)**

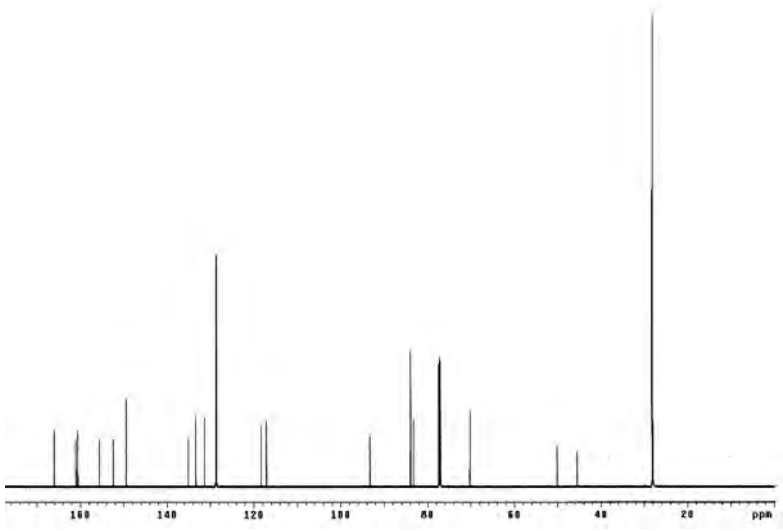

**G∧C base**

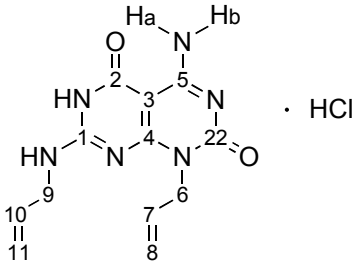


· HCl

**$^{1}$H–NMR (600 MHz, DMSO-*d*$_6$)**

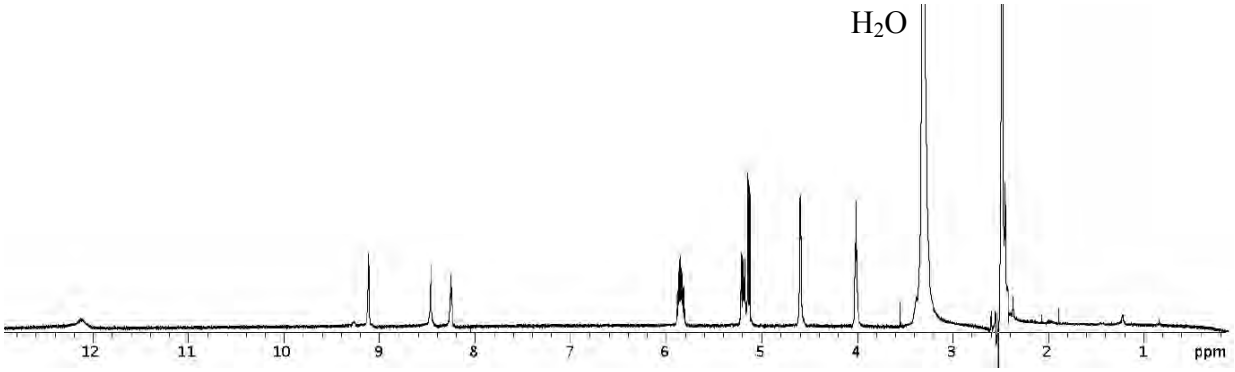


**$^{13}$C–NMR (150 MHz, DMSO)**

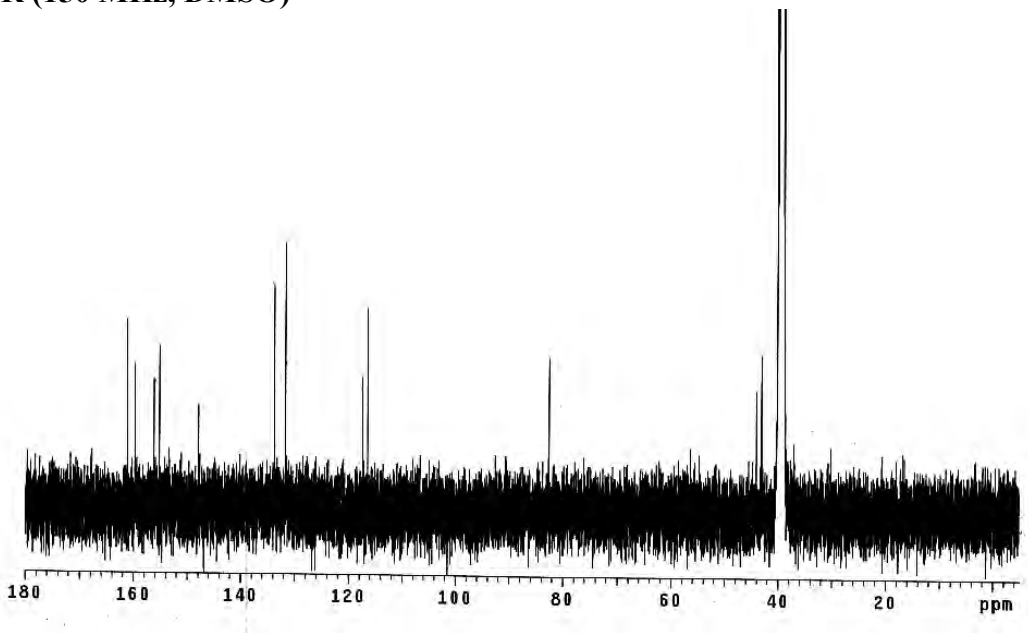

# Single Crystal x-Ray Structure

CCDC639261 (CIF file attached)

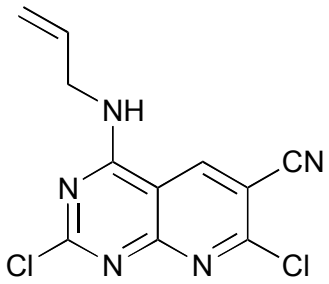


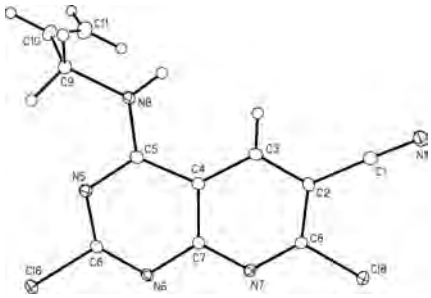

## SEM Imaging

SEM was performed using a high resolution Hitachi S–4800 or S–5500 cold field emission gun SEM. All SEM images were obtained without staining, at 5 kV accelerating voltage and a working distance of 3.0 mm (Figure S1). Samples were prepared by floating a carbon–coated 400–mesh copper grid on a droplet of G∧C or ×G∧C (see figure captions for concentration used) for 30 s. The grid was then blotted with filter paper and dried in air for 1 day prior to imaging. We thank Dr. Shunya Watanabe (Hitachi High Technologies, Naka Application Centre) for recording some of the SEM images on the Hitachi S5500.

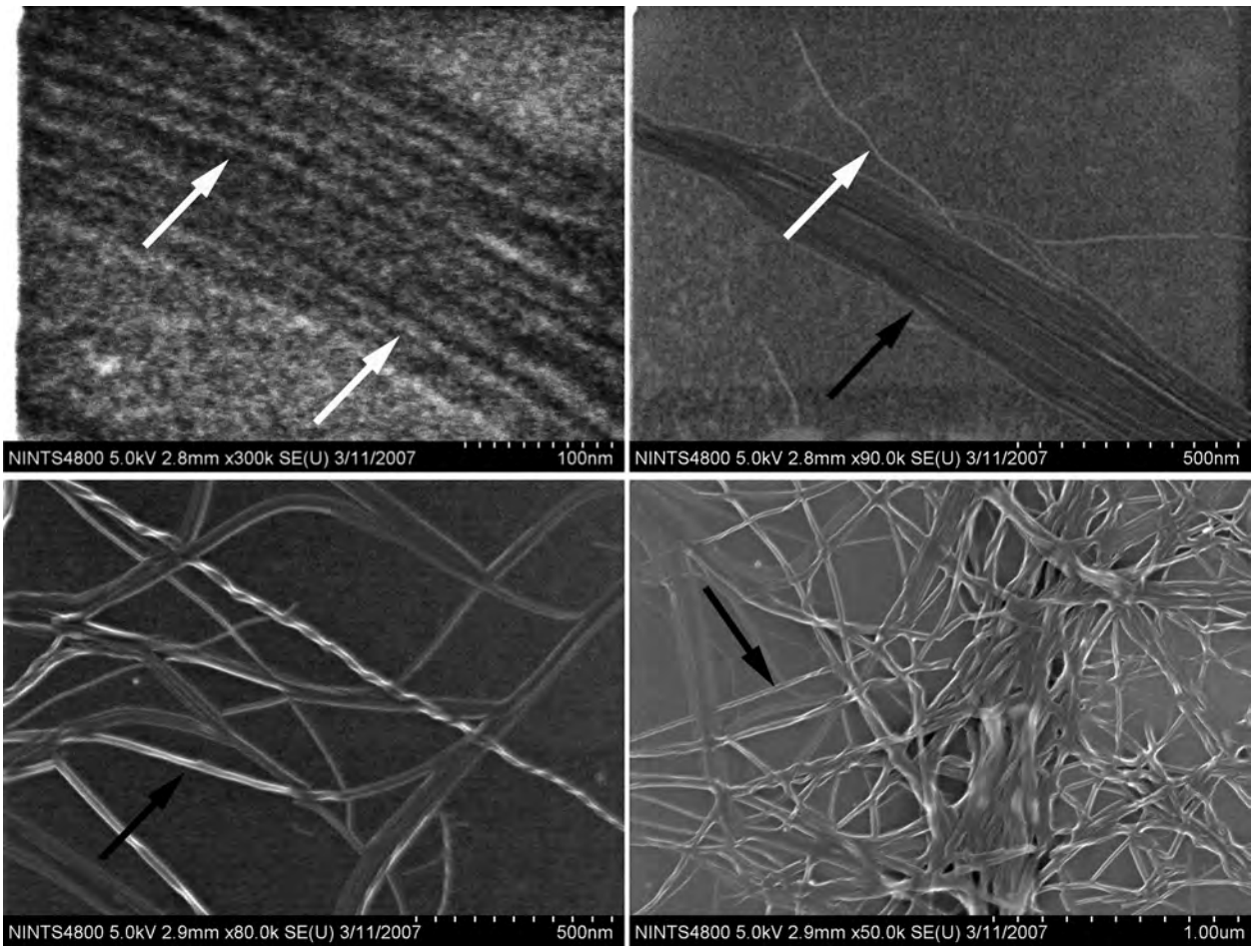


**Figure S1.** SEM images of G∧C (0.2 mg/mL in DMF) recorded on Hitachi S4800. The white arrows point at single RNTs and the black arrows point at ribbons and bundles of RNTs.

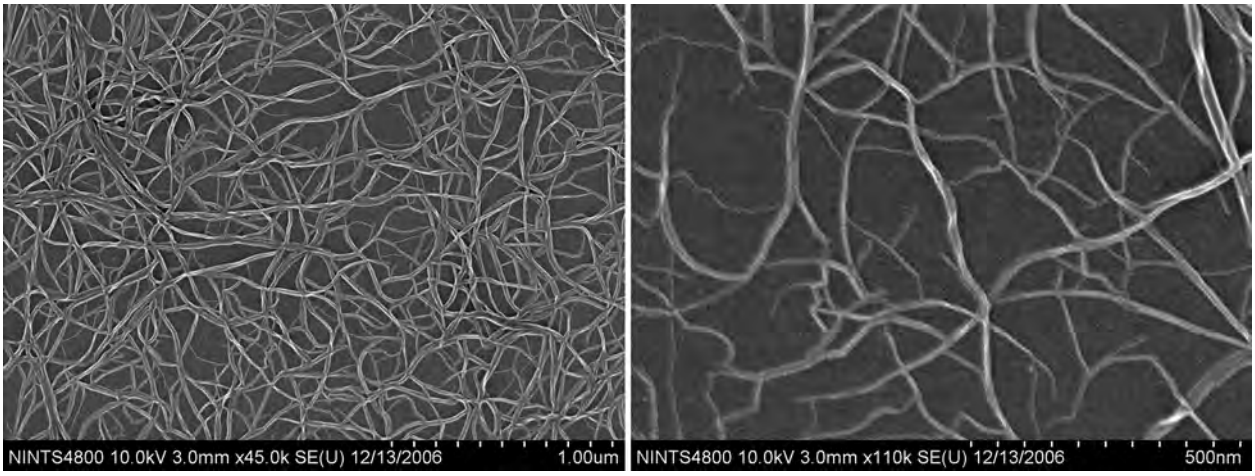


**Figure S2.** SEM images of G∧C (1 mg/mL in DMF) recorded on Hitachi S4800.

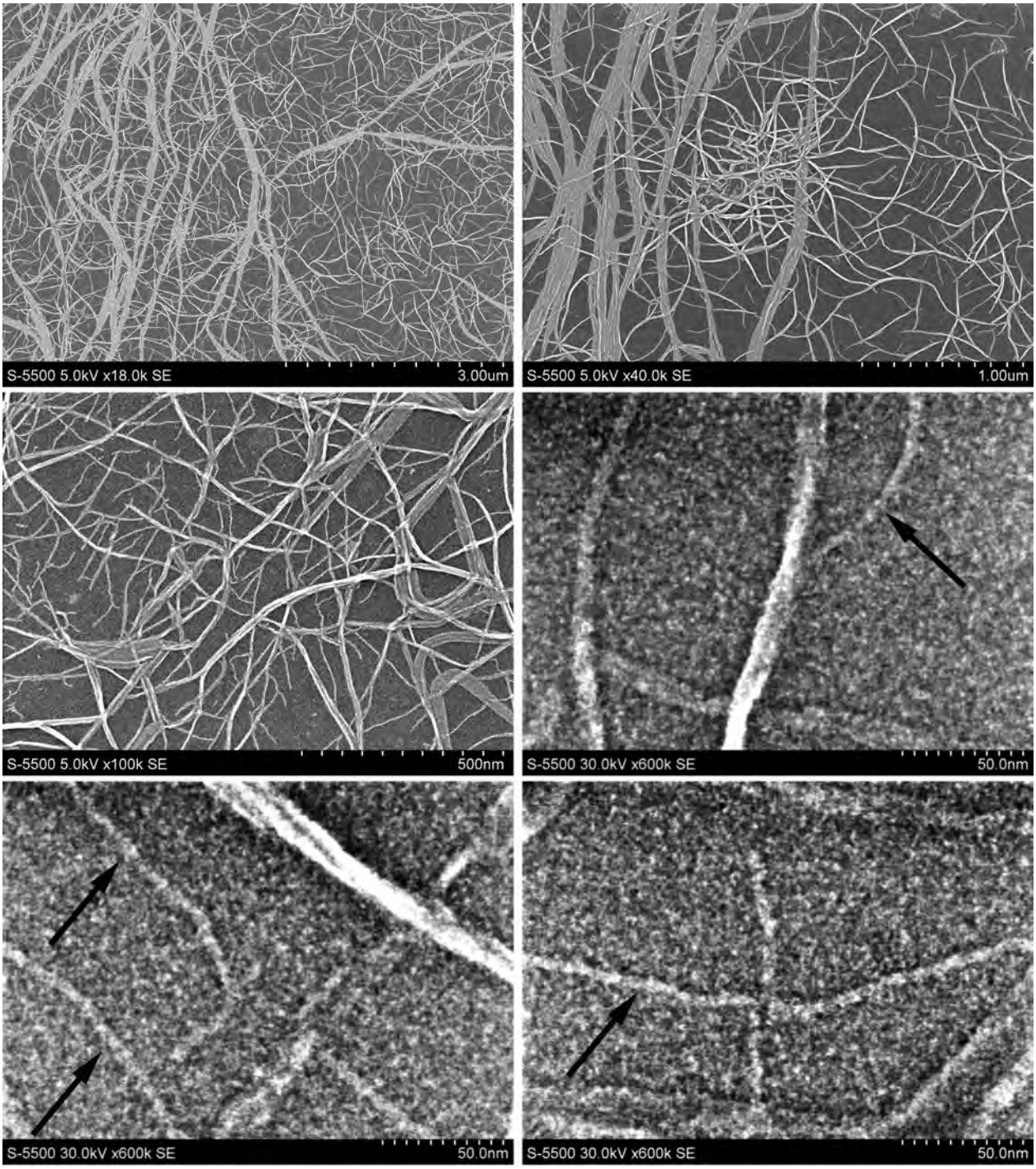


**Figure S3.** SEM images of G∧C (0.3 mg/mL in DMF) recorded on Hitachi S5500. The black arrows point at individual RNTs.

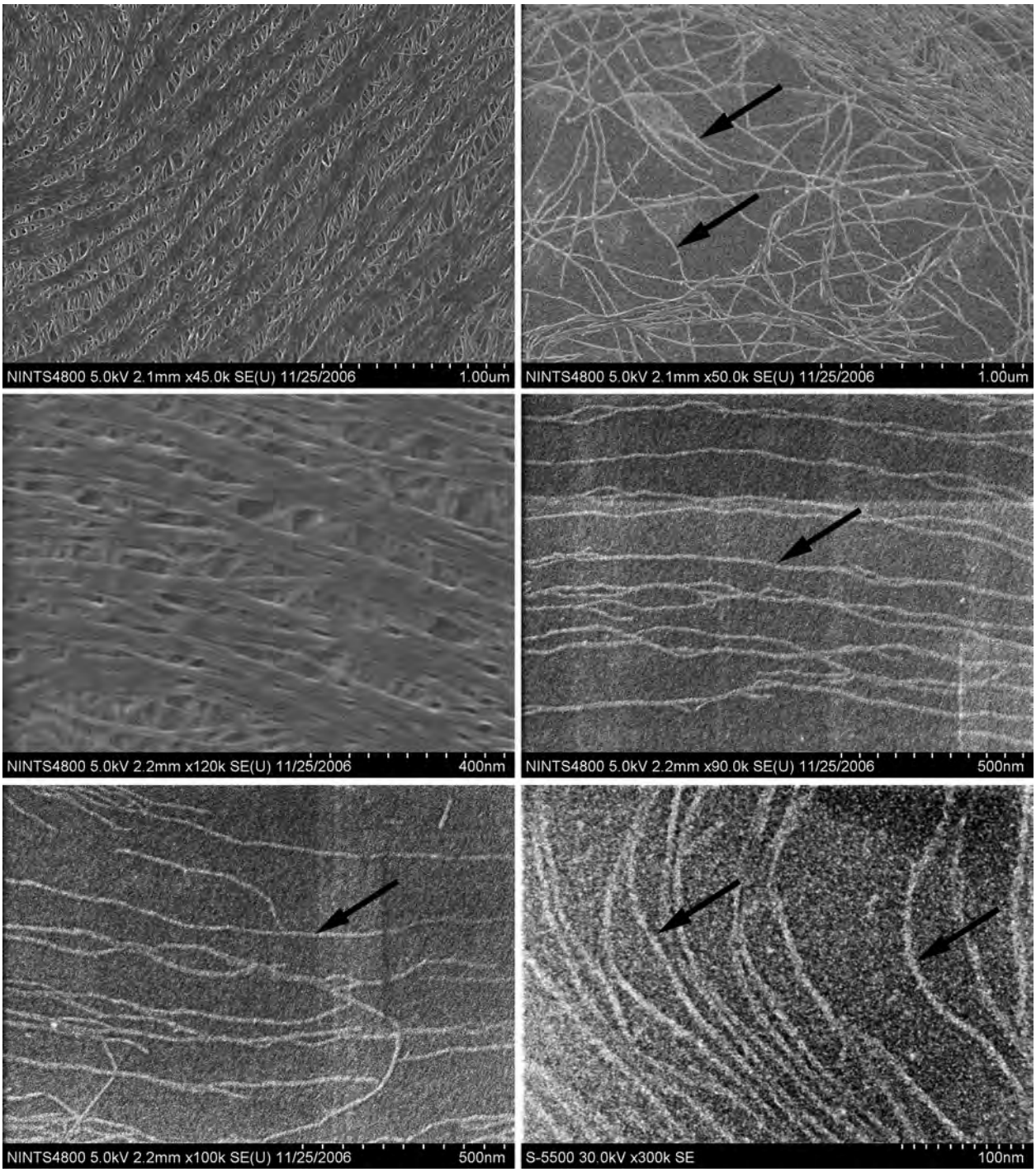


**Figure S4.** SEM images of ×G∧C (0.3 mg/mL in DMF) recorded on Hitachi S4800 or S5500. The black arrows point at individual RNTs.

## AFM Imaging

AFM measurements were performed in tapping mode (TM–AFM) at a scan rate of 0.5–1 Hz per line and amplitude setpoint of 1 V using a Digital Instruments/Veeco Instruments MultiMode Nanoscope IV equipped with an E scanner. Silicon cantilevers (MikroMasch USA, Inc.) with low spring constants (4.5 N/m) were used in tapping mode (TM–AFM). Clean mica substrates (1 × 1 $cm^2$) were prepared and the RNT samples were deposited by spin–coating 0.2–0.3 mg/mL solution at 2000 rpm for 20 s.

Molecular modeling was performed to predict the inner and outer diameters of the G∧C and ×G∧C RNTs (see Molecular Modeling section). The inner/outer diameters were calculated to be 1.0/3.1 nm and 1.4/3.5 nm for G∧C and ×G∧C RNTs, respectively. Over 400 measurements were obtained for each sample and the values obtained were plotted in Figure S7. For the ×G∧C RNTs, the distribution centered around 3.6 ± 0.3 nm, whereas for the G∧C RNTs the distribution centered around 2.2 ± 0.2 nm. While for the ×G∧C RNTs the measured and calculated diameters (i.e. height profile) were in excellent agreement, for the G∧C RNTs the AFM height measurements (2.2 ± 0.2 nm) were consistently ~1 nm lower than the corresponding calculated diameter (3.1 nm). This result suggests that the G∧C RNTs are mechanically far more compressible than the ×G∧C RNTs.[3]

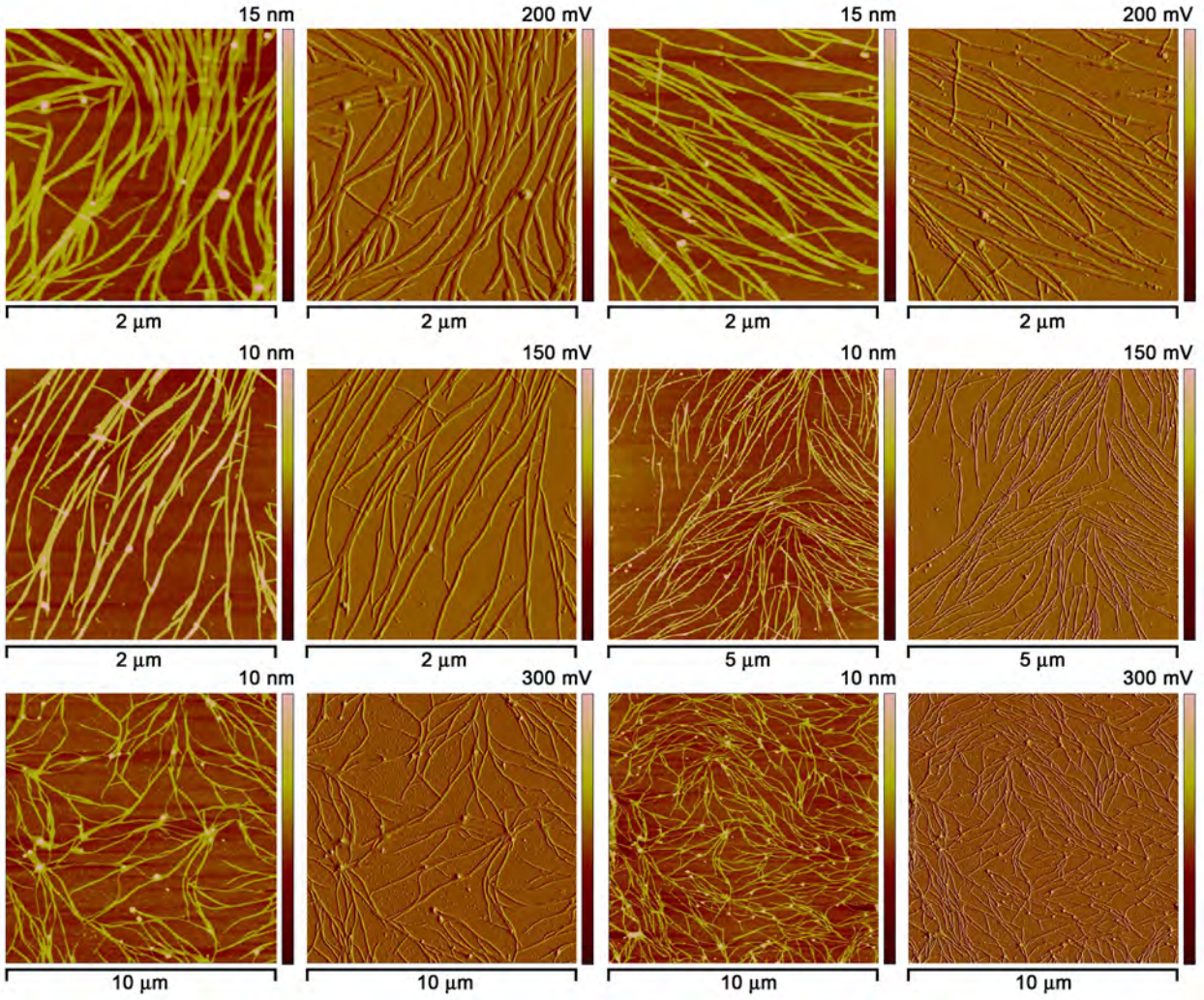


**Figure S5.** TM–AFM height and amplitude images of ×G∧C RNTs (0.2 mg/mL, 0.6 mM in DMF).

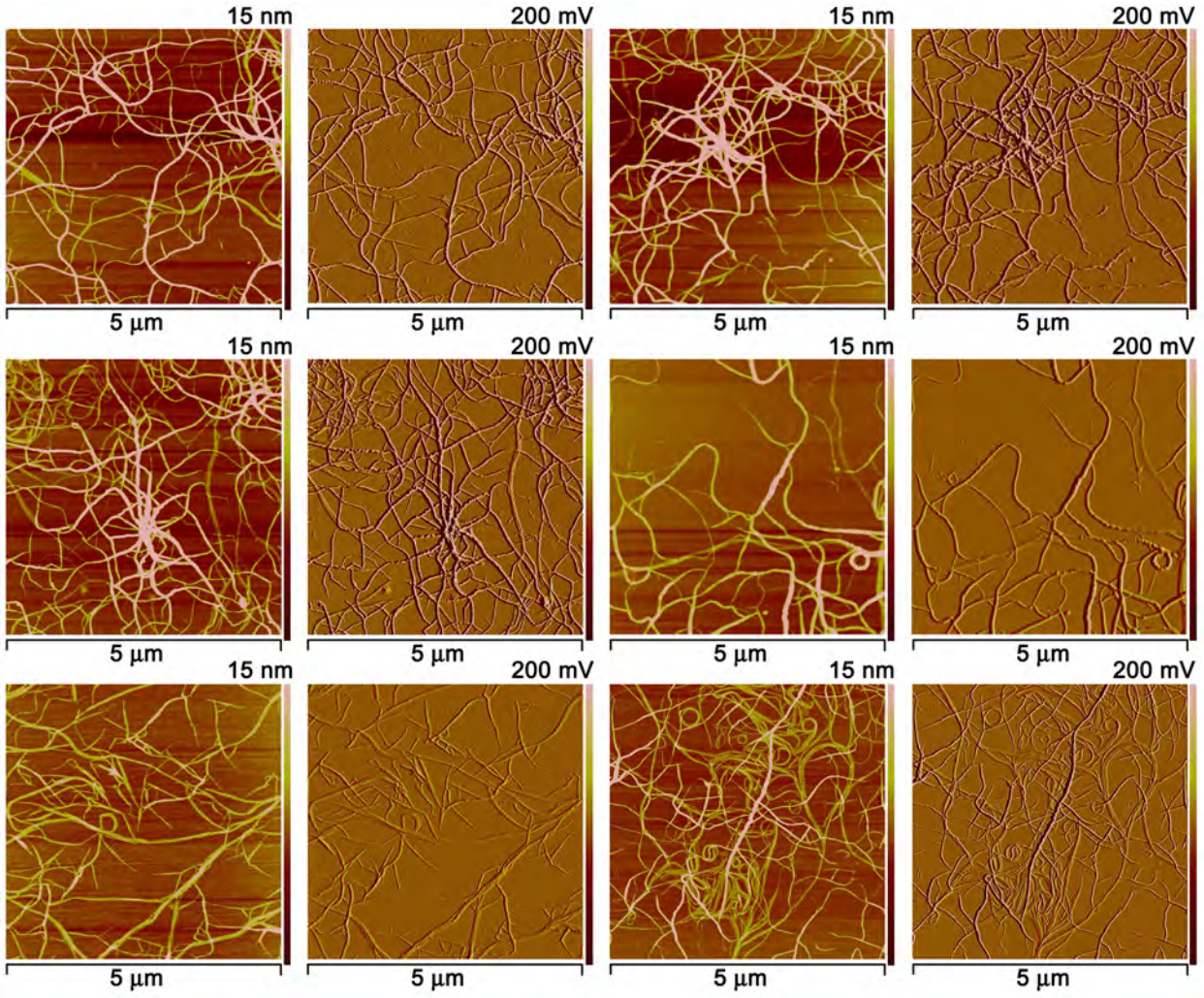


**Figure S6.** TM–AFM height and amplitude images of G∧C RNTs (0.3 mg/mL, 1.1 mM in DMF).

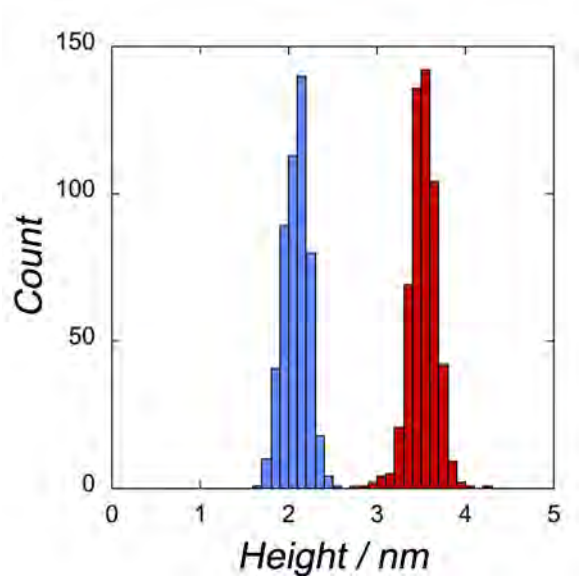


**Figure S7.** Histogram showing the AFM height distributions (i.e. measured diameters) of G∧C (blue) and ×G∧C (red) RNTs. The bin size is 0.1 nm.

## TEM Imaging

TEM images were recorded on a JOEL 2010 microscope operated at 200kV using a $LaB_6$ tip. The samples were prepared by dissolving ×G∧C (0.2 mg/mL, 0.6 mM) and G∧C (0.3 mg/mL, 1.1 mM) in DMF. The solutions were heated to ~100°C and allowed to cool to room temperature for 1 h. Aliquots (10 μL) of each solution were placed on a 400 mesh ultra-thin carbon coated TEM grid (EM Sciences) for 10 s before excess material was blotted with filter paper. All the samples were air-dried for 24 h at room temperature. The grids were placed inside a staining chamber (40 mL vial) containing a 4% $OsO_4$ aqueous solution in a 5 mL vial (Sigma Aldrich) and sealed overnight. Samples were then removed from the staining chamber and placed in a fume hood for 3 h before imaging. This staining method was not effective for the G∧C sample, which was then incubated overnight in a small vial with $OsO_4$ crystals. The ×G∧C samples stained more readily and to a larger extent than the G∧C samples, as evidenced by the increased contrast observed on the nanotubes. This difference was attributed to the possibility for coordination with the pyridyl nitrogen and to a reduced functional group density of the ×G∧C RNTs surface.

Pixel-to-pixel measurements were made on images taken at 250,000× direct magnification or higher using Adobe Photoshop CS2. 129 measurements were made over 26 images on the ×G∧C sample, which was found to have an average diameter of 3.6 ± 0.2 nm (3.58 ± 0.13 nm). 172 measurements were made over 52 images on the G∧C sample, which was found to have a diameter of 3.1 ± 0.2 nm (3.07 ± 0.15 nm). These results established that the ×G∧C RNTs are, as anticipated, 0.5 nm wider than G∧C RNTs.

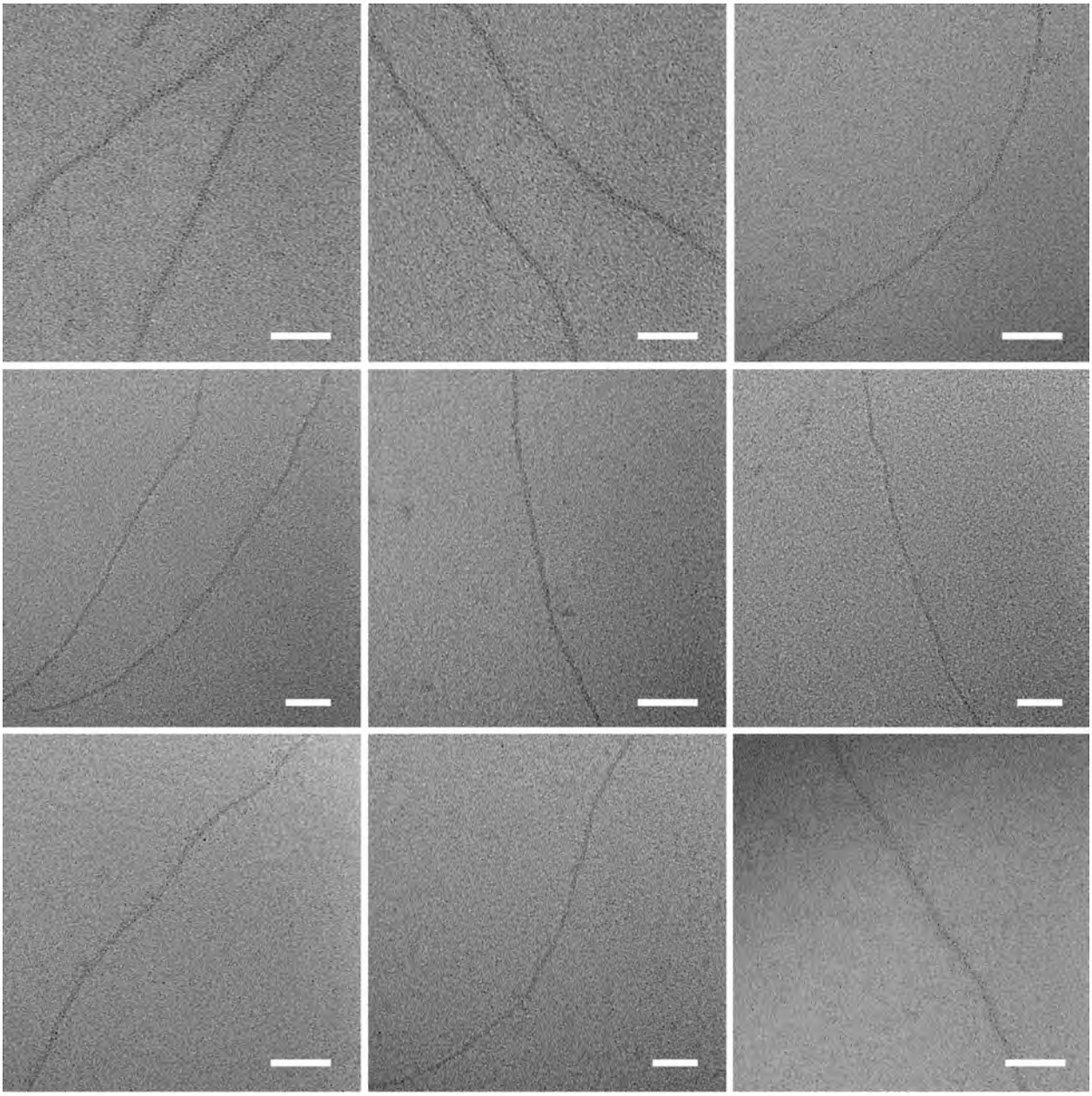

**Figure S8.** TEM images of G∧C RNTs (scale bars = 40 nm).

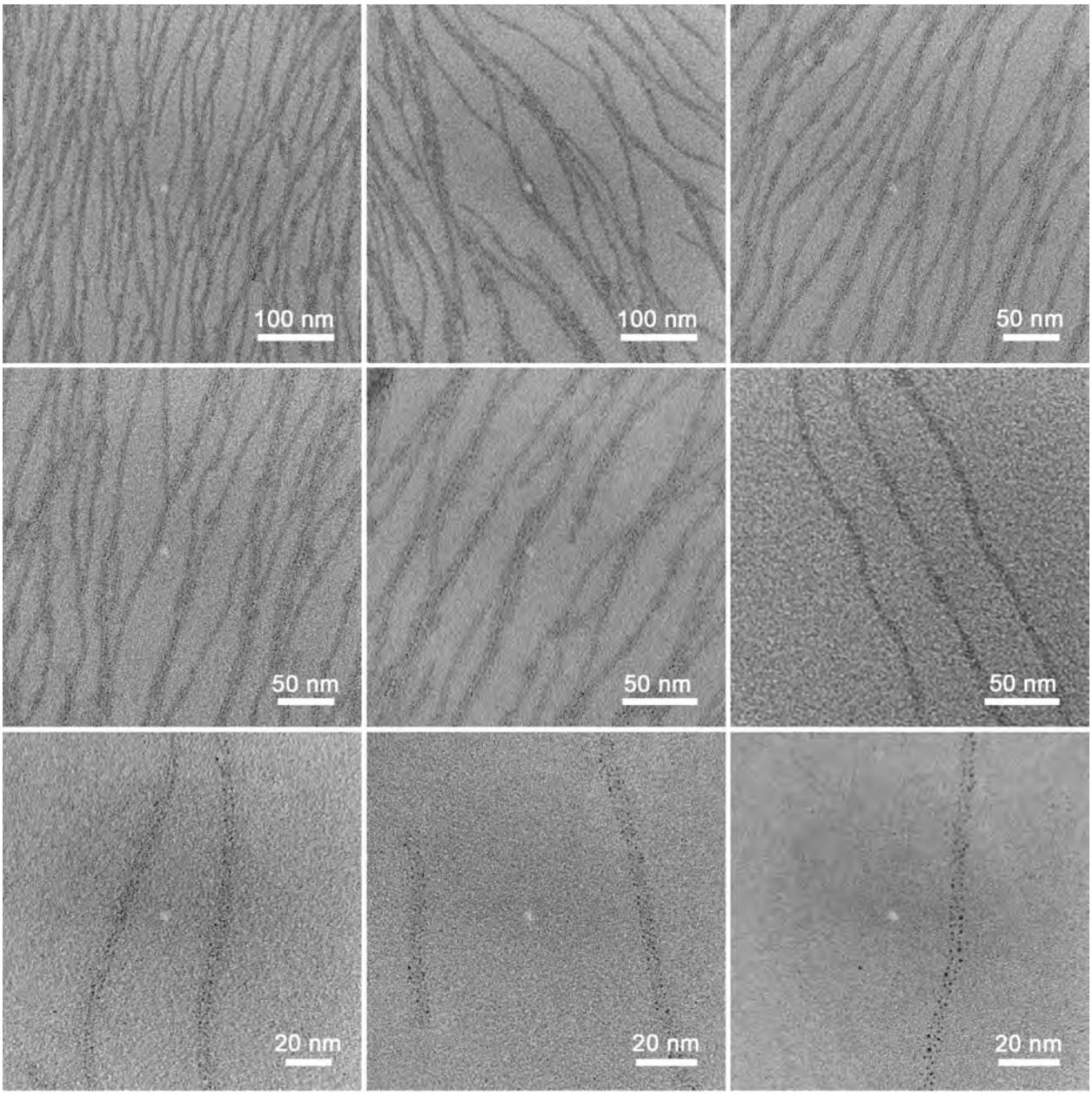


**Figure S9.** TEM images of ×G∧C RNTs.

## Molecular Modeling

To predict the outer and inner diameters of ×G∧C and G∧C nanotubes, we performed a conformational search in both DMSO and DMF as follows:

**Step 1: Conformational search.** The motif was first minimized, then 64 conformers were generated by varying dihedral angles around two bonds in increments of 45° (Figure S10).

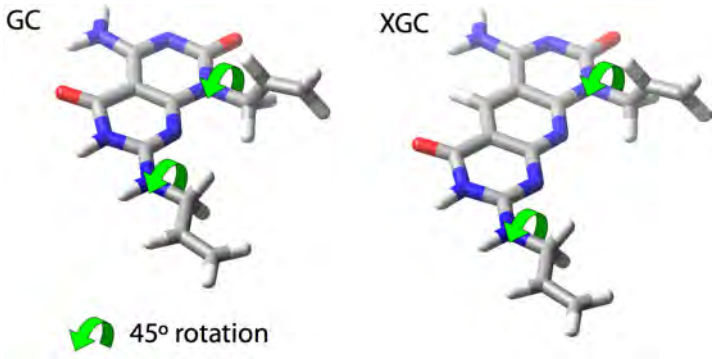


**Figure S10.** Conformers of G∧C and ×G∧C modules generated by varying the dihedral angles around 2 bonds as indicated by the curved arrows.

**Step 2: Formation of the RNTs.** Each of the 64 non–optimized conformers were multiplied and arranged to form a six–fold symmetry rosette maintained by 18 H–bonds. The rosettes were then stacked in a tubular fashion with inter–planar distance of 4.5 Å and a rotation angle of 30° per rosette along the main axis. This arrangement was based on previous work done on similar systems.[1,3a,4]

**Step 3: Energy minimization of the RNTs.** Molecular models for the RNTs were generated using Macromodel 8.5. The RNT interaction models employed the OPLS–AA force field. The PRCG energy minimization was then applied to the 64 RNTs consisting each of 9 rosettes, with the top and bottom 2 rosettes as well as all the G∧C/×G∧C bases fixed to reduce end effects. The

central rosette in each of the optimized 64 RNTs was then taken to construct RNTs composed of N=1–15 rosettes.

**Step 4: Solvation free energy.** To obtain the thermodynamic stability of RNTs in DMSO and in DMF, we employed the three–dimensional reference interaction site model (3D–RISM) integral equation complemented with the Kovalenko–Hirata (KH) closure approximation.[5] The 3D–RISM–KH integral equation theory of molecular solvation explicitly and properly accounts for the effect of chemical specificities of the RNTs, and DMSO and DMF solvents. This theoretical method based on first principles of statistical mechanics provides a detailed microscopic insight into the organization of solution molecules both outside and inside the RNT, and their role in RNT formation.[4c-4d]

The solvation structure is given by the probability density of finding site α of solvent molecules at position r around the solute molecule, $\rho_\alpha g_\alpha(\mathbf{r})$, which is determined by the average number density $\rho_\alpha$ of solvent site α in the solution bulk and the 3D distribution function $g_\alpha(\mathbf{r})$ of solvent site α, or normalized probability density, showing site density enhancement ($g_\alpha>1$) or depletion ($g_\alpha<1$) relative to the average density at a distance from the solute (where $g_\alpha \rightarrow 1$).

The 3D–RISM integral equation is written as

$$h_\gamma(\mathbf{r}) = \sum_\alpha c_\alpha(\mathbf{r}) * \chi_{\alpha\gamma}(r), \qquad (1)$$

where $h_\gamma(r)$ is the 3D total correlation function of site γ related to the 3D distribution function by $g_\gamma(r)=h_\gamma(r)+1$, and $c_\gamma(r)$ is the 3D direct correlation function which has the asymptotics of the solute–solvent site interaction potential: $c_\gamma(r)\sim -u_\gamma(r)/(k_BT)$; $\chi_{\alpha\gamma}(r)$ is the site–site susceptibility of pure solvent; the site indices α and γ enumerate all sites on all sorts of solvent molecules, and "*" denotes convolution in the direct space. The other relation between the 3D total and direct

correlation functions were employed to complement the 3D–RISM integral equation (1) in the 3D–KH closure:

$$g_\gamma(\mathbf{r}) = \begin{cases} \exp(d_\gamma(\mathbf{r})) & \text{for} \quad d_\gamma(\mathbf{r}) \le 0 \\ 1 + d_\gamma(\mathbf{r}) & \text{for} \quad d_\gamma(\mathbf{r}) > 0 \end{cases} \qquad (2)$$

$$d_\gamma(\mathbf{r}) = -\frac{u_\gamma(\mathbf{r})}{k_B T} + h_\gamma(\mathbf{r}) - c_\gamma(\mathbf{r}),$$

where $u_\gamma(r)$ is the 3D intermolecular interaction potential between the whole solute and solvent site γ specified by the molecular force field, and $k_BT$ is the Boltzmann constant times the temperature of the solution.

The site–site susceptibility of solvent breaks up into the intra– and inter–molecular terms,

$$\chi_{\alpha\gamma}(r) = \omega_{\alpha\gamma}(r) + \rho_\alpha h_{\alpha\gamma}(r), \quad (3)$$

where the intramolecular correlation function, or intramolecular matrix $\omega_{\alpha\gamma}(r)=\delta_{\alpha\gamma}+(1-\delta_{\alpha\gamma})\delta(r-l_{\alpha\gamma})/(4\pi l_{\alpha\gamma}^2)$ represents the geometry of solvent molecules with the site–site separations $l_{\alpha\gamma}$ specified by the molecular force field, and $h_{\alpha\gamma}(r)$ is the radial total correlation function between sites α and γ in pure solvent. In advance of the 3D–RISM–KH calculation, the site–site correlation functions $h_{\alpha\gamma}(r)$ of pure solvent are obtained from the dielectrically consistent RISM theory coupled with the KH closure (DRISM–KH), applied to the bulk solvent. The bulk solvent susceptibility (3) is then input into the 3D–RISM integral equation (1).

The solvation free energy of the solute supramolecule in solvent obtained from the 3D–RISM–KH integral equations (1) and (2) is given by the closed analytical expression

$$\mu_{\text{solv}} = k_B T \sum_\gamma \rho_\gamma \int d\mathbf{r} \left[ \frac{1}{2} h_\gamma^2(\mathbf{r}) \Theta(-h_\gamma(\mathbf{r})) - c_\gamma(\mathbf{r}) - \frac{1}{2} h_\gamma(\mathbf{r}) c_\gamma(\mathbf{r}) \right], \quad (4)$$

where the site index γ enumerates all sites on the solvent molecule, and $\Theta(x)$ is the Heaviside step function,

$$\Theta(x) = \begin{cases} 1 & \text{for} \quad x \geq 0 \\ 0 & \text{for} \quad x < 0 \end{cases} \quad .$$

The 3D–RISM–KH theory was applied to the 9 (G∧C module) and 15 (×G∧C module) RNTs composed of N rosettes (N = 1–15) in DMSO or DMF. The densities of 1.0957 and 0.9443 $cm^3$/mol were used for DMSO and DMF, respectively, and the temperature was 25ºC. The dielectric constants of 48.75 and 37.59 were used for DMSO and DMF, respectively. The free energy of a given RNT conformer was obtained as a sum of the internal energy and the solvation free energy $\mu_{solv}$ given by Equation (3). Figures S11–S14 present the free energy trajectories showing that the most stable conformers are #25 and #31 RNTs for the G∧C and #22 and #43 RNTs for the ×G∧C RNTs in both DMSO and DMF solvents. The conformations are shown in Figures S15–S18.

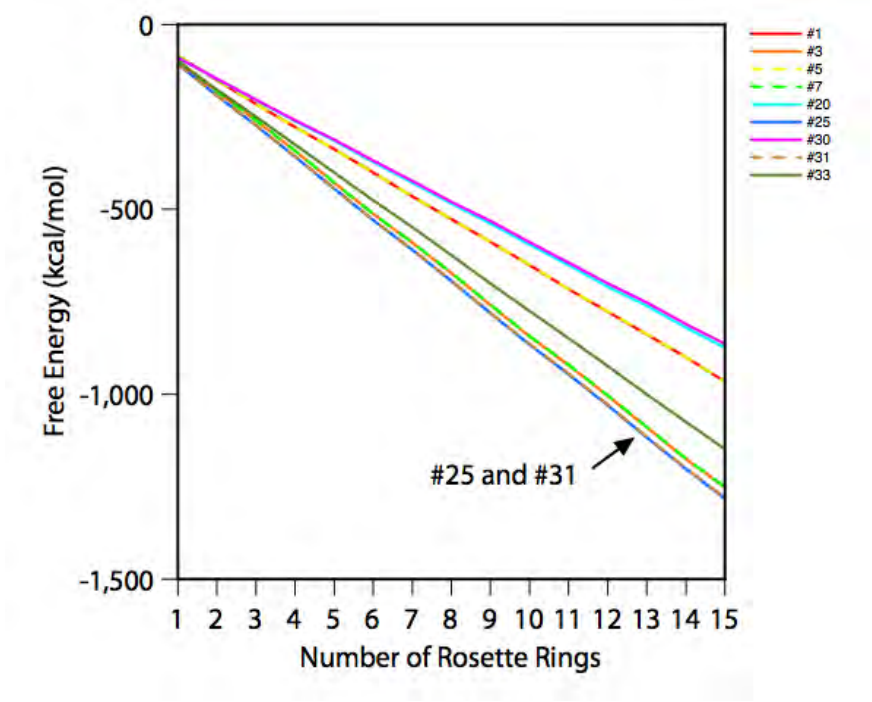


**Figure S11.** Free energy trajectories of the nine most stable G∧C–based RNTs in DMSO.

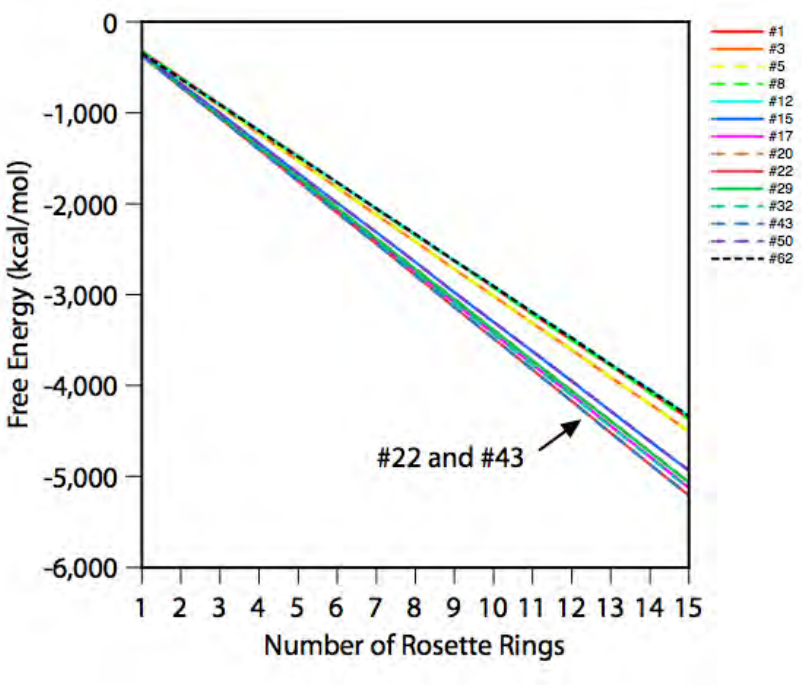


**Figure S12.** Free energy trajectories of the sixteen most stable ×G∧C–based RNTs in DMSO.

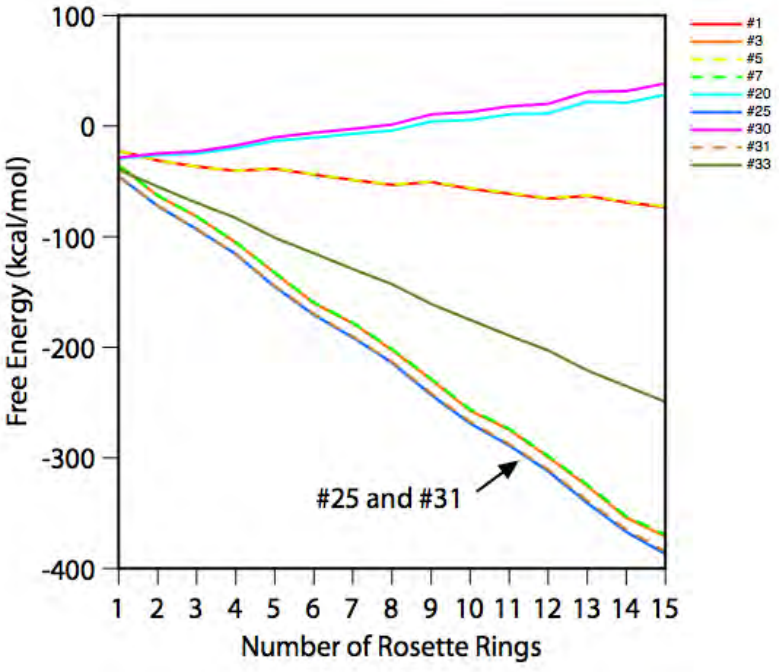


**Figure S13.** Free energy trajectories of the nine most stable G∧C–based RNTs in DMF.

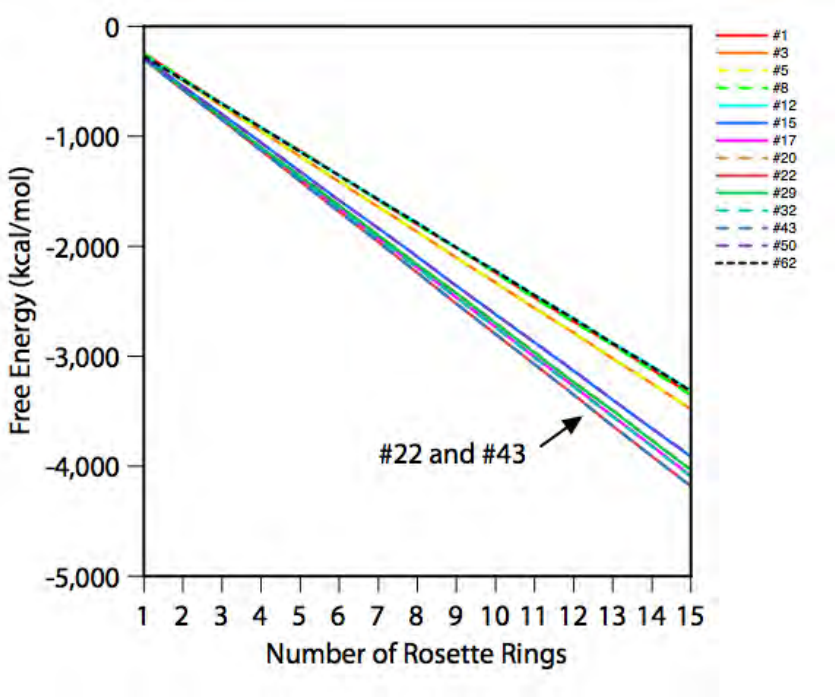


**Figure S14.** Free energy trajectories of the sixteen most stable ×G∧C–based RNTs in DMF.

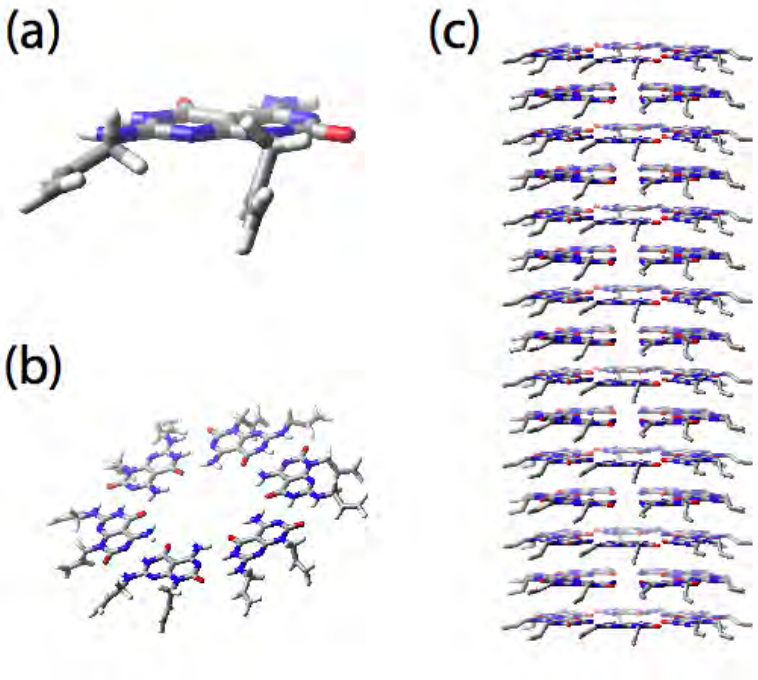


**Figure S15.** (a) Motif (b) rosette, and (c) RNT for G∧C–based RNT #25.

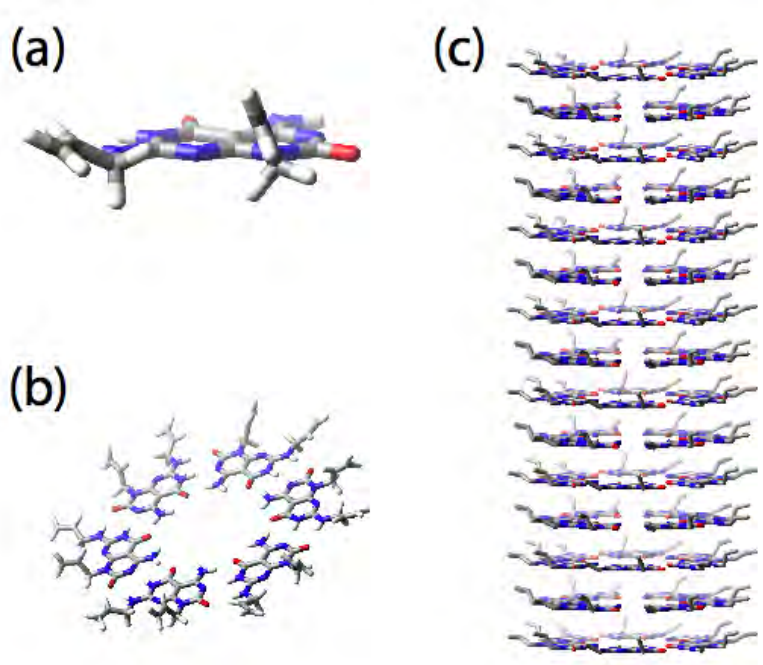


**Figure S16.** (a) Motif (b) rosette, and (c) RNT for G∧C–based RNT #31.

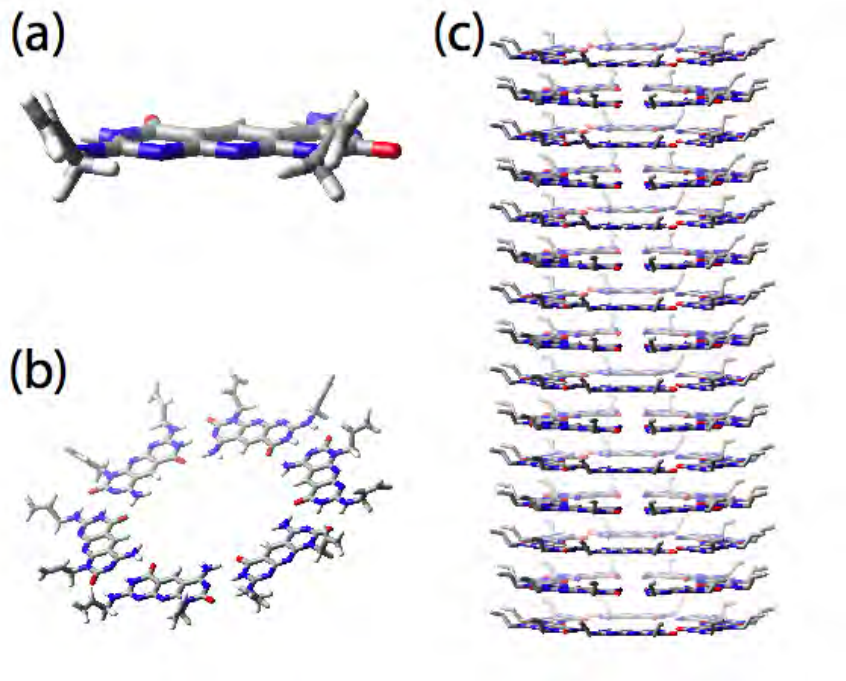


**Figure S17.** (a) Motif (b) rosette, and (c) RNT for ×G∧C–based RNT #22.

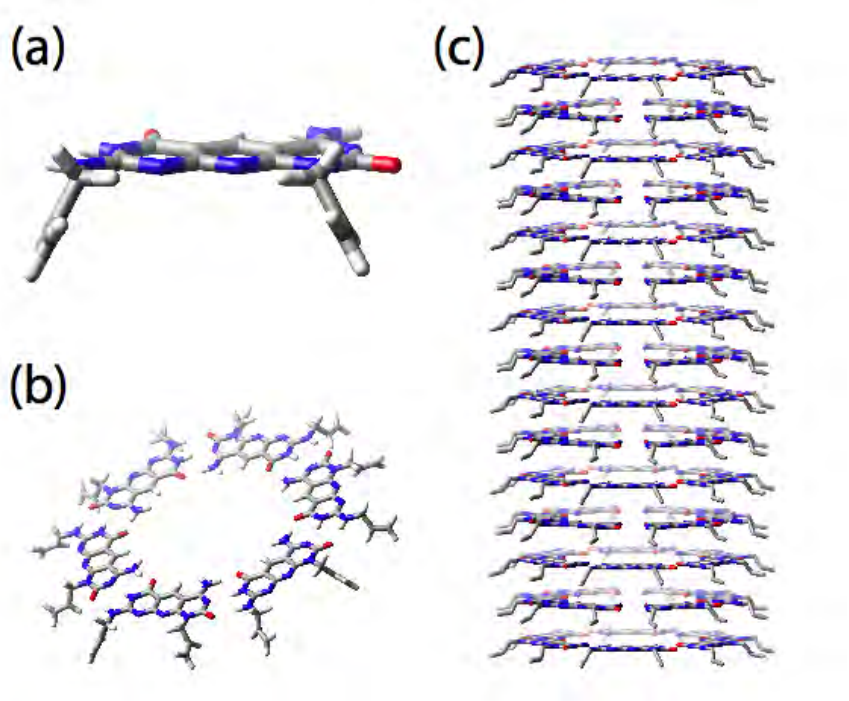


**Figure S18.** (a) Motif (b) rosette, and (c) RNT for ×G∧C–based RNT #45.

**Molecular dynamics simulations**

MD simulations were run in Amber10[6] using GAFF[7] for ×G∧C motif and guest molecules, dexamethasone and tamoxifen, and TIP3P water model.[8] The partial charges for the ×G∧C motif and the guest molecules were assigned based on OPLS-AA force field.[9,10] The RNT structure composed of 10 rosette rings was constructed based on the most stable conformation #22 (Figure S17), and the guest molecules were placed inside the RNT channel. This host-guest system is used as the initial structure for the simulation. The starting structures were solvated in 5406 and 5402 water molecules for RNT-dexamethasone and RNT-tamoxifen systems, respectively. One chloride anion was added to the RNT-tamoxifen system to neutralize the system. The solvent molecules were equilibrated under 1 bar at 25°C during the 3 ns simulation with the stepwise decrease of positional restraint for the RNT-guest molecule. The final structure obtained from this simulation was used as the starting configuration for the 5 ns simulation under 1 bar at 25°C

with no positional restraints for the RNT-guest molecule. Temperature was controlled by Langevin dynamics with the collision frequency of 1 $ps^{-1}$, and pressure was regulated by the pressure relaxation time of 2 ps. A cutoff of 10-Å was used for non-bonded interactions, and long-range electrostatic interactions were treated wit the particle-mesh Ewald method.[11] A 1 fs time step was used.

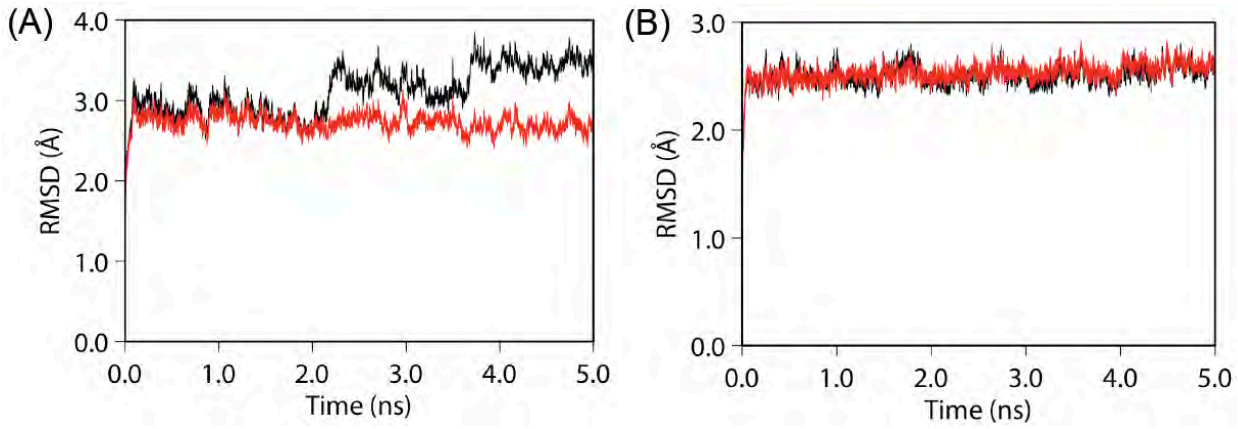


**Figure S19.** RMSD of RNT with respect to the initial structure as a function of simulation time.

Figure S19 presents the root mean square deviation (RMSD) of RNT with respect to the initial structure as a function of simulation time, (A) for RNT-dexamethasone system and (B) for RNT-tamoxifen system. The black line shows the RMSD of the heavy atoms in RNT and the red line indicates that in the middle part of RNT (RNT except top and bottom rings). Although the RNT conformation is fluctuating from the initial structure, the convergence of RMSD for the middle part of RNT (red line), which mainly holds the guest molecule, suggests that the middle part of RNT has been smoothly equilibrated with holding the guest molecule. The small change can be seen at around 2 ns from the black line in Figure S19A. This change is because one of the motifs in the top rosette ring started fluctuating largely at that point and most likely it is the end effect. However, the fluctuation of this motif in the top rosette ring seems not to affect the encapsulation of the dexamethasone molecule inside the RNT channel (see Figure S20).

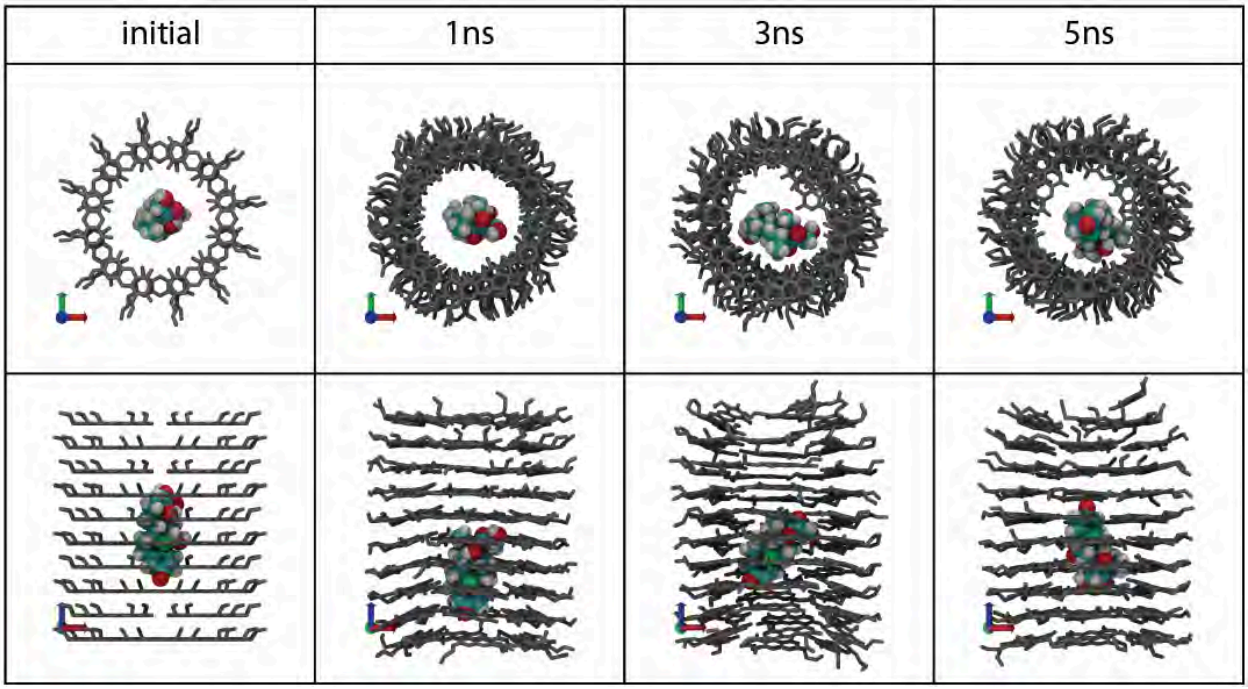


**Figure S20.** Initial structure and snap shots from the MD trajectory for RNT-dexamethasone system.

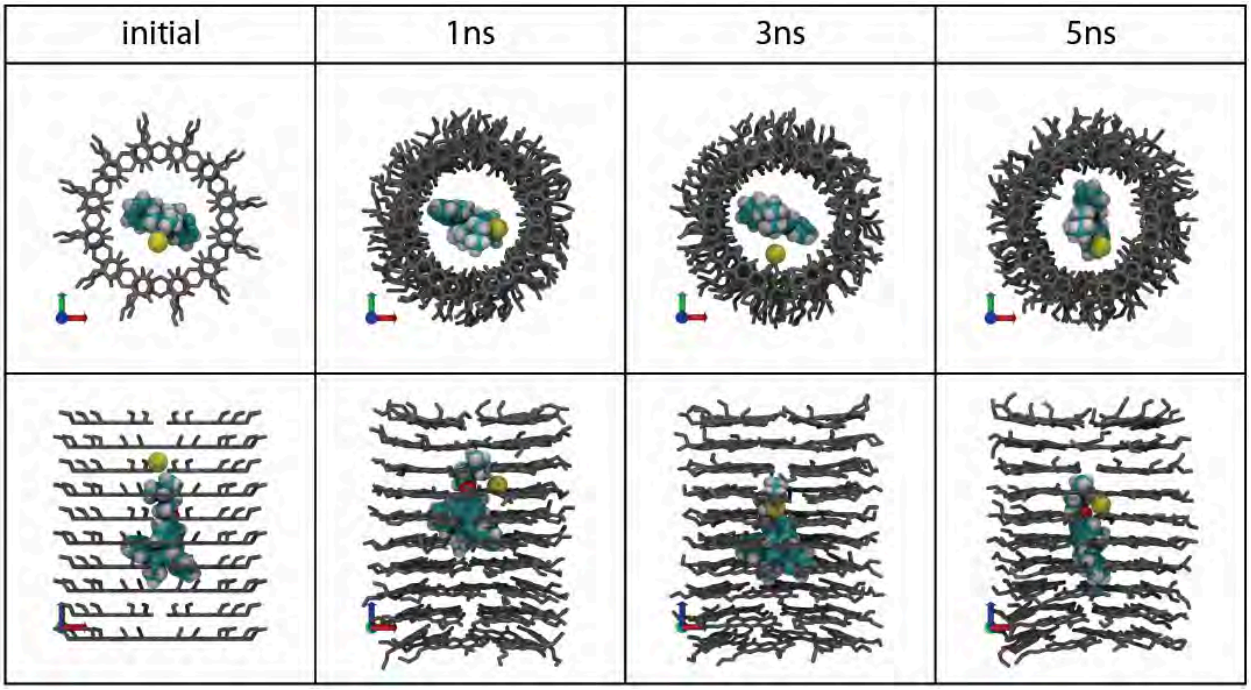


**Figure S21.** Initial structure and snap shots from the MD trajectory for RNT-tamoxifen system.

Figure S20 and Figure S21 present the initial structure and snapshots from the MD trajectory at 1, 3, 5 ns. The water molecules as well as the hydrogen atoms of RNT are omitted for clarity. The RNT is colored in grey. The carbon, oxygen, nitrogen, hydrogen, and fluorine atoms of guest molecules are colored in cyan, red, blue, white, and green. The $Cl^-$ counter ion for the tamoxifen is colored in yellow. This preliminary MD simulation strongly supports the ability of ×G∧C–RNT to encapsulate small hydrophobic drugs.

**References**

1. Fenniri, H.; Deng, B. L.; Ribbe, A. E.; Hallenga, K.; Jacob, J.; Thiyagarajan, P. *Proc. Nat. Acad. Sci. USA* **2002**, *99*, 6487–6492.
2. Borzsonyi, G.; Oderinde, S.; Beingessner, R. L.; Deng, B.–L.; Yamazaki, T.; McDonald, R.; Kovalenko, A.; Fenniri, H. *Helv. Chim. Acta* **2009**, *92*, 1963–1972.
3. (a) Moralez, J. G.; Raez, J.; Yamazaki, T.; Motkuri, K.; Kovalenko, A.; Fenniri, H. *J. Am. Chem. Soc.* **2005**, *127*, 8307–8309. (b) Knez, M.; Sumser, M. P.; Bittner, A. M.; Wege, C.; Jeske, H.; Hoffmann, D. M. P.; Kuhnke, K.; Kern, K. *Langmuir* **2004**, *20*, 441–447.
4. (a) Fenniri, H.; Mathivanan, P.; Vidale, K. L.; Sherman, D. M.; Hallenga, K.; Wood, K. V.; Stowell, J. G. *J. Am. Chem. Soc.* **2001**, *123,* 3854–3855; (b) Fenniri, H.; Deng, B.–L.; Ribbe, A. E. *J. Am. Chem. Soc.* **2002**, *124*, 11064–11072; (c) Johnson, R. S.; Yamazaki, T.; Kovalenko, A.; Fenniri, H. *J. Am. Chem. Soc.* **2007**, *129*, 5735–5743. (d) Yamazaki, T.; Fenniri, H.; Kovalenko, A. *ChemPhysChem* **2010**, *11*, 361-367.
5. A. Kovalenko, in *Molecular Theory of Solvation*, ed. F. Hirata, Kluwer Academic Publishers, Dordrecht, 2003, vol.24, pp.169-275.
6. Case, D. A.; Darden, T. A.; Cheatham, T. E., III; Simmerling, C. L.; Wang, J.; Duke, R. E.; Luo, R.; Crowley, M.; Walker, R. C.; Zhang, W.; Merz, K. M.; Wang, B.; Hayik, S.; Roitberg, A.; Seabra, G.; Kolossváry, I.; Wong, K. F.; Paesani, F.; Vanicek, J.; Wu, X.;

Brozell, S. R.; Steinbrecher, T.; Gohlke, H.; Yang, L.; Tan, C.; Mongan, J.; Hornak, V.; Cui, G.; Mathews, D. H.; Seetin, M. G.; Sagui, C.; Babin, V.; Kollman, P. A. AMBER 10; University of California, San Francisco, 2008.

7. Wang, J.; Wolf, R. M.; Caldwell, J. W.; Kollman, P. A.; Case, D. A. *J. Comput. Chem.* **2004**, *25*, 1157–1174.
8. Jorgensen, W. L.; Chandrasekhar, J.; Madura, J. D.; Impey, R. W.; Klein, M. L. *J. Chem. Phys.* **1983**, *79*, 926–935.
9. Jorgensen, W. L.; Maxwell, D. S.; Tirado-Rives, J. *J. Am. Chem. Soc.* **1996**, *118*, 11225–11236.
10. McDonald, N. A.; Jorgensen, W. L. *J. Phys. Chem. B* **1998**, *102*, 8049–8059.
11. Darden, T.; York, D.; Pedersen, L. *J. Chem. Phys.* **1993**, *98*, 10089–10092.